NTNU

Norwegian University of
Science and Technology

Scaling of Calcium Carbonate at Heated Surfaces in a Continuous System

Margrethe Nergaard

Chemical Engineering and Biotechnology
Submission date: June 2011
Supervisor: Jens-Petter Andreassen, IKP
Co-supervisor: Ralf Beck, IKP

Norwegian University of Science and Technology
Department of Chemical Engineering

Preface

Contrary to what many believe, fulfilling a master's is not done isolated in a lab, hidden in a dark basement, where you do not talk to anyone before the thesis is delivered. If so was, this thesis would never been born ☺

I would first of all thank my main advisor, associate professor Jens-Petter Andreassen, for introducing me to the awesome world of crystallization, believing in and backing me whenever that has been necessary. Your always-open-door, irrespective of the scientific degree of the topic to be discussed, has been highly appreciated. My co-advisor, post.doc Ralf Beck, deserve a great thank for all help, patience and support inside as well as and outside the lab. I would also thank engineer Julian Tolchard for all help with the SEM and XRD analyzes and PhD-student Karen Nessler Seglem for proofreading and valuable inputs.

My family does also deserve some glory: Even though you have limited scientific understanding of my area of specialization, no one is better at nodding and replying that yes, my crystals are pretty. Julie, my sweet niece, deserves a special thank just for giving auntie a perfect excuse to escape from school now and then. At last, I have to thank all my fantastic girls; you make life outside the lab so worth all the hours spent inside the lab.

This Master Thesis' was written on behalf of the Department of Chemical Engineering (IKP) at the Norwegian University of Science and Technology (NTNU) during 20 weeks spring 2011. I hereby declare that this work is done independently and in accordance with the exam regulations at NTNU.

Trondheim, 24.06.2011

Margrethe Nergaard

Abstract

Scaling is the precipitation of a mineral layer on a surface. Sparingly soluble salts with inverse solubility, which calcium carbonate exhibits, will prefer precipitation at heated surfaces, making heat exchangers a target for scale formation.

A continuous setup was used to study scale formation, the nature of the scale formed and scaling rate. An internally heated U-shaped tube was inserted into a continuously stirred tank, giving the same conditions for all scaling points. The experimental setup allowed the supersaturation to be constant throughout the experiment.

An onset of scale formation was found around $S_{calcite}$~4.5 for a tube surface temperature of 90°C. The surface was first covered with an introductory scale layer before outward directed dendritic growth took place.

The deposited mass increased by 35% when the temperature of the heated tube was increased from 50°C to 90°C. At tube temperature 50°C, 43% calcite and 56% aragonite was formed. As temperature was increased to 70°C and above, more than 97% of the scale layer was aragonite. Less vaterite than predicted by literature was found.

Increasing the supersaturation increased the amount of scale formed. A linear relationship between supersaturation and deposited mass was identified. However, this is not expected to be valid for all ranges of supersaturations due to the correlation between growth mechanisms and supersaturation. Increasing the bulk temperature when the tube temperature was constant had little impact on the deposited mass, but changed the morphology towards a more porous and fragile structure.

Extensive bulk nucleation occurred at high supersaturations. The effective steady state supersaturation in close vicinity to the heated surface was reduced from the initial by almost 130% for the high supersaturation, compared to 35% for the lower. This points towards a threshold in supersaturation; above this, bulk nucleation will consume most of the excessive supersaturation introduced to the system.

Scale growth rate for aragonite at high supersaturation (S=20) was experimentally determined to the range of 1.2E-5 and 1.6E-5 kg/m^{2}s. For the lower supersaturation (S=6), a constant scale growth rate of 3.5E-6 kg/m^{2}s was found.

By assuming a density of the scale layer, linear growth rates of ~22 nm/s and 5 nm/s for S=20 and S=6 respectively, were obtained. These were compared to linear growth rates of aragonite from batch experiments.

The morphology and polymorphism of the scale being was investigated by Scanning electron microscope (SEM) and powder X-ray diffraction (XRD), respectively.

Table of contents

1 Introduction

A crystal is a solid substance with a regular arrangement of constituents into a lattice (Mullin, 2001). When crystallizing, ions can constitute themselves into various arrangements creating different polymorphs of the same compounds. For crystals to nucleate and grow, the solvent must be supersaturated by the solute. The supersaturation can be manipulated by changing temperature, composition or pH, as all these parameters change the activity of the crystallizing ions.

Scaling is the precipitation of a mineral layer, usually of a sparingly soluble compound, on a surface. It is also referred to as precipitation fouling or simply just fouling. The precipitation results from, among others, changes in fluid composition, pH or physical parameters such as temperature and pressure. Scaling represents a serious problem for the oil and gas industry. Scale formation can occur in the reservoir to give pressure drops and blocked reservoir pores, leading to reduced productivity. Scale can also form along pipelines, in the bulk fluids, in most parts of the processing system and in the worst case, on security equipment (Crabtree et al., 1999).

Calcium carbonate is one of the most common scale forming minerals. It crystallizes in three different anhydrous polymorphs; vaterite, aragonite and calcite, named in order of increasing stability. The polymorphs have different growth regimes and growth rates. In industrial processes, heat exchangers represent potential targets for scale formation. A heat exchanger transfers heat from a warm stream to a colder stream through a solid wall. Calcium carbonates exhibits inverse solubility, thus favoring precipitation at elevated temperatures as a result. Scale on heat exchanger surfaces can restrict flow, reduce the heat transfer and thereby the efficiency of the heat exchanger, increase the energy costs and potentially cause formation of hot spots. Control or prevention of scaling represents both an economic and environmental advantage.

The mentioned challenges make scaling an unpredictable process, creating headaches for unfortunate engineers. A striking quote taken from (Karabelas, 2002) states: "It is impossible at present to predict (with a satisfactory degree of reliability) the temporal variation of fouling resistance which is the relevant parameter for engineering calculations".

Morphology, polymorphism, growth regimes and growth rates are important for scale build-up and effective scale-inhibition (Flaten et al., 2009). Morphology and growth regimes have been thoroughly studied over the last decades, but most experiments have been conducted as batch experiments. For most industrial processes where scaling at heated surfaces is a problem, such as heat exchange, the system is continuous rather than a batch. The flow is usually large and the system at steady state, making loss of dissolved species due to

precipitation negligible, compared to the bulk concentration. Hence, the composition can be considered to be constant. This is in contrast to fluid flowing in a well or along a very long pipe, where the supply of reactants can be limited and conditions change with position.

Some continuous tests for studying scale formation exist, where the most common is the so-called tube blocking test. In this test, reactants flow through a long, thin steel pipe heated from the outside. The pressure difference across the tube is monitored. Buildup of scale will eventually block the tube, resulting in increased pressure. From the time required to block the tube and the thickness of the scale, scaling rate can be determined (Bazin et al., 2005), (Zhang et al., 2001). As mentioned, the tube block test is terminated when the pressure increase indicates blockage. However, for a long test tube, the blockage might occur in one section of the tube only, whereas other parts of the tube are still scaling. As the supersaturation is consumed along the tube length, both the change in supersaturation and the experiment length are averaged over the tube. Morphology and scaling regimes are sensitive to variations in the scaling parameters (Andritsos et al., 1997) and a system where total scaling is studied gives no information of the different scaling parameters for each scaling point along the tube. This makes the tube block test less suitable for studying the correlation between growth rates, growth regime and morphology.

The motivation for this work is to study scaling in an environment where the scaling conditions are constant for the whole scaling area throughout the experiment. In order to fully understand the scaling process, control over scaling parameters is a prerequisite. The work is based on specialization project conducted by the author fall 2010. In this project, an experimental setup with continuous flow of reactants and constant supersaturation was designed. Also, the setup allowed the temperature of the scaling surface and the bulk fluid to be controlled separately, making it possible to control the scaling parameters. The same setup is used in this work.

Various combinations of scaling parameters such as composition of the feed (i.e. inlet supersaturation), temperature of the scaling surface and temperature of the bulk solution are studied systematically. The objective is to study the correlation between supersaturation and the onset of scale formation and also when bulk nucleation becomes noteworthy. For supersaturations where surface scaling is the dominating mechanism, the amount of scale and the scaling rates are determined and coupled with existing data in literature. Emphasis is put on investigating the scaling nature such as surface coverage, polymorphism, morphology and growth directions of the scale layer. The morphology and polymorphism of scale and bulk precipitated particles is investigated by SEM and powder-XRD, respectively.

2 Theory

In this section, theory on crystalline matter, nucleation and growth of crystals and the calcium carbonate system will be presented. Further, theory relevant for scale formation and scale growth will be introduced to the extent this is available. Ending the section, some attention is given to basic concepts on heat exchangers and stirred reactors.

2.1 Terms and definitions

Within the field of deposits on surfaces, a wide range of different terms are used. "Scaling" is a general term referring to the deposition of solid material, often minerals, at a surface, from an aqueous solution (Cowan and Weintritt, 1976). Scale formation can take place for example downhole an oil field, along a pipe or in process equipment (Zhang et al., 2001), (Wu et al., 2009) and is not limited to surfaces where a heat gradient is present.

To describe scaling at heated surfaces, another term widely used is "fouling". Bott (1995) defines fouling as "accumulation of unwanted deposits from a moving fluid on the surface of a heat exchanger." Neither of the general terms, scaling and fouling, differentiates between adhesion of deposits that are pre-formed and formation of deposits in-place close to or at the surface.

"Crystallization fouling" and "precipitation fouling" are sometimes used to describe the specific process of formation of a crystalline matter from solution directly on site at the deposition surface (Bott, 1997),(Andritsos and Karabelas, 2003). Corresponding, "particulate fouling" can be used to describe the process of adhesion of pre-formed crystal (Fahiminia et al., 2007). In these contexts, the term "crystal" is not limited to aqueous systems, but can also describe deposits of wax crystals in petroleum production (Bott, 1997).

Throughout this work, "scaling" will refer to the formation of a crystalline matter from solution directly on site at a surface. To differentiate clearly, "particulate deposition" will be used on adhesion of solid particles formed in the bulk solution and transported to the surface.

2.2 Crystalline matter

A crystalline material is characterized by atoms situated in a repeating array over large atomic distances. Amorphous material is material without such an order; it is randomly packed molecules. The way the atoms, ions or molecules are spatially arranged, is referred

to as the crystal structure and will define some of the properties of the crystalline solid. It is common to divide the atomic structure into small repeating units called unit cells, which represent the symmetry of the crystal structure. Unit cells are usually parallelepipeds or prisms with three sets of parallel edge lengths and three interaxial angels. A total of seven different combinations of these parameters exist, each representing a distinct crystal system (Mullin, 2001).

When a material has more than one crystal structure, is is called polymorphism. The different polymorphs can have different appearance, morphology, at macro scale as a result of the local environment where the polymorph grows. A crystal where the repeated arrangement of atoms is extended throughout the entire structure without interruption is called a unit crystal. Most crystalline matters, however, are polycrystalline, meaning it consists of many small crystals or grains with different crystallographic orientation (Callister, 2007).

Even though crystals are classified in seven crystallographic systems, large variations (modifications of habit) in the relative size of each face of a given crystal exist. Rapid growth in one direction gives for example elongated growth resulting in a needle-shaped crystal. The degree of supersaturation and agitation of the system can influence the crystal habit (Mullin, 2001).

Crystalline defects, irregularities from the repeating structure, are present in all crystalline matter. The defects can be classified as point defects or line defects. Point defects impact only one local area of the unit cell, whereas a line defect will cause the whole structure to be misaligned. Where an extra plane (or portion of such) exists, a defect occurs where the edge of this plane terminates inside the crystal. This is called an edge dislocation. Another type of line defect is the screw dislocation, which is formed by an applied shear stress. It results in a part of the crystal being shifted one atomic distance relative to the rest of the crystal. Screw dislocation together and twinning (explained later) is illustrated in Figure 1 below.
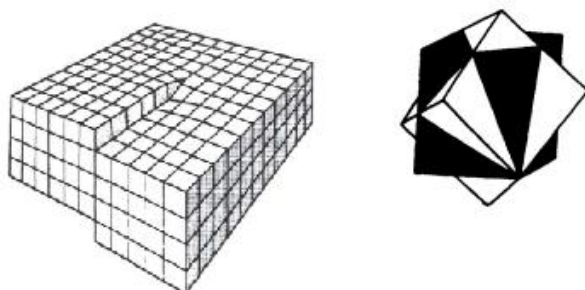

Figure 1: Screw dislocation (right), twin crystals appearing to pass through each other (left) (Mullin, 2001)

4

In the border between the crystal grains of a polycrystalline matter, interfacial defects can occur. These defects have two dimensions and separate the regions of the crystalline material with different crystallographic orientation. A special case of such a grain boundary is a twin boundary. Here, the atoms are joined with mirror symmetry on each side of the boundary (Callister, 2007). It is possible for twins to have the appearance of one individual passing through the other.

2.3 Thermodynamics

2.3.1 The Driving Force

The fundamental driving force for crystallization is the difference between the chemical potential of a substance in solution and in solid state. This can be written as

$$\Delta\mu = \mu_c - \mu_s \tag{2.1}$$

Here, μ_s and μ_c are the chemical potentials of a molecule in the solution and in the crystal, respectively. If $\Delta\mu > 0$, a driving force for crystallization is established and nucleation and crystal growth can occur. The chemical potential is defined by the standard chemical potential, μ_0, and the relation between activity, a, temperature, T, and the universal gas constant, R, as

$$\mu = \mu_0 + RT\ln a \tag{2.2}$$

For a system where the solution is saturated by solute, we may express the fundamental driving force with dimensionless variables as

$$\frac{\Delta\mu}{R \cdot T} = \ln\left(\frac{a}{a^*}\right) = \ln S \tag{2.3}$$

where a^* is the activity of the saturated solution and S the fundamental supersaturation ratio based on activities. An established driving force for crystallization then corresponds to S>1. The activity is related to the concentration, c, through the experimentally dependent activity coefficient, γ,

$$a = \gamma c \tag{2.4}$$

The activity coefficient is a measure of the solutions deviation from ideality. Thus, in an ideal solution the activity coefficient will equal 1 and the activity and concentration will be equal. Replacing activities by concentrations is a valid approximation for very dilute systems, but also commonly used in the industry (Mullin, 2001).

2.3.2 Electrolyte solutions

For electrolyte solutions the interactions between the ions can be significant even at very low concentrations (Helbæk and Kjelstrup, 2006). In order to account for these interactions, the mean ionic activity, $a_{\pm}$, is often used. It is given as

$$a = a_{\pm}^{\nu}$$

(2.5)

where $\nu = (\nu_{+} + \nu_{-})$ is the number of moles of ions in one mole solute. The mean ionic activity can also be defined in terms of the ion activity product (IAP) as

$$a_{\pm} = \left(IAP\right)^{\frac{1}{\nu}} = \left(a_{+}^{\nu+} \cdot a_{-}^{\nu-}\right)^{\frac{1}{\nu}}$$

(2.6)

The supersaturation ratio can then be expressed in terms of IAP and the activity product at equilibrium; the solubility product, K_{sp}:

$$S = \left(\frac{IAP}{K_{sp}}\right)^{\frac{1}{\nu}}$$

(2.7)

Now, by using Equation(2.7), Equation (2.3) can be rearranged into

$$\frac{\Delta\mu}{R \cdot T} = \nu \cdot \ln S$$

(2.8)

where the number of ions are accounted for through the term ν.

The activity of a given ion cannot be measured directly. In addition, since the electrochemical potentials of ions in solution cannot be separated, a mean ion activity coefficient, $\gamma_{\pm}$, has to be used for electrolytes (Helbæk and Kjelstrup, 2006). This coefficient can be related to measurable quantities and thus calculated through various models. For very dilute solutions, the Debye-Hückel Equation can be used:

$$\gamma_{\pm} = -\left|z_{+}\right| \cdot \left|z_{-}\right| \cdot A \cdot \sqrt{I} = -\left|z_{+}\right| \cdot \left|z_{-}\right| \cdot A \cdot \sqrt{\left(\frac{1}{2} \cdot \sum_{i} c_{i} \cdot z_{i}^{2}\right)}$$

(2.9)

Here, z is the charge number, c the concentration, A a solvent-dependent proportional coefficient and I the ionic strength. For systems of high ionic strength or very sparingly soluble salts, other models must be used in order to find the mean ion activity coefficient.

2.4 Nucleation

After a supersaturated system is established, a number of small molecular clusters of the new crystalline phase, must be formed (Kashchiev and van Rosmalen, 2003). This process, known as nucleation, has two main mechanisms, as illustrated in Figure 2 below.
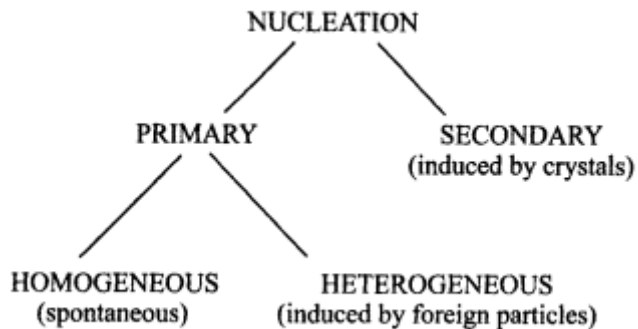

Figure 2: Classification of nucleation (Mullin, 2001)

Primary nucleation is nucleation in a solution where crystalline matter of the same compound not is present, as opposed to secondary nucleation in which nucleation is induced by such solute crystals. Primary nucleation is further divided into homogeneous and heterogeneous nucleation. Homogeneous nucleation occurs in an ideally pure solution constituted by solvent and solute molecules only. Heterogeneous nucleation takes place in the presence of impurities, foreign particles or substrates that can provide centers for nucleation.

At low supersaturations, the supersaturation itself may not be enough to induce crystallization. Ostwald first used the expressions "labile" and "metastable" to differentiate between supersaturation ratio levels where nucleation would occur or not. This is illustrated in Figure 3 below. Here, the solid black line represents the equilibrium line and the dotted line the transient border between the metastable and labile regions (Mullin, 2001).
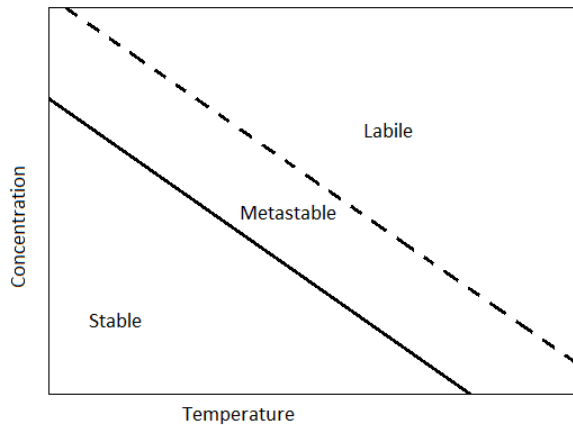
Figure 3: Solubility - supersolubility diagram illustrating at which combinations of temperature and concentration nucleation and growth can occur. In the labile regime the supersaturation is high enough for nucleation to occur. In the metastable zone, only growth will take place. In the stable regime, the solution is no longer supersaturated and preformed crystals will dissolve

2.4.1 Homogeneous nucleation

In homogeneous nucleation, solutions with sufficient high supersaturation forms unstable molecular clusters due to Brownian motions (Mullin, 2001). These clusters continue to form and redissolve themselves until enough ions have been added for the cluster to reach a certain critical size. At this size, the change in free energy, ΔG, associated with the nucleation process is maximized. Any extra addition of ions will lower the free energy, promoting further nucleation and growth.

For homogeneous nucleation of a spherical particle, the nucleation rate can be written as

$$J = A \cdot \exp\left(-\frac{16\pi\gamma^3 v^2}{3k^3 T^3 \left(\ln S\right)^2} \right)$$

(2.10)

A is a kinetic parameter affected by the diffusion coefficient, level of supersaturation, temperature and the interfacial tension (Mullin, 2001). Further, γ is the interfacial tension, v the molar volume, k the Boltzmann constant and S the supersaturation. Equation (2.10) defines that the supersaturation, temperature and interfacial tension are the three variables controlling the nucleation rate.

2.4.2 Heterogeneous nucleation

In the presence of a foreign object, nucleation can be induced at supersaturations lower than the ones required for homogeneous nucleation. Hence, the change in free energy for

heterogeneous nucleation, ΔG_{het}, must be lower than the corresponding change in free energy for homogeneous conditions, ΔG.

As stated in Equation (2.10), the interfacial tension impacts the rate of nucleation. When introducing a foreign surface, this new surface can have a smaller interfacial tension between the crystallizing object and the surface, γ_{cs}, and the corresponding tension between the crystallizing object and the liquid, γ. 3D-nucleation refers to nucleation where the crystallizing body grows in three dimensions, as shown as a capped sphere in Figure 4a.
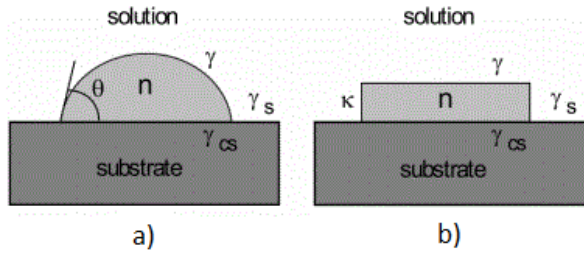

Figure 4: 3D (a) and 2D (b) heterogeneous nucleation (Kashchiev and van Rosmalen, 2003)

The contact angle, θ, can be expressed by the Young Equation as

$$\cos\theta = \frac{\gamma_s - \gamma_{cs}}{\gamma}$$

(2.11)

This Equation states that for 0°<θ<180°, the foreign surface will be wetted by the crystallizing object. This gives $\Delta G_{het}<\Delta G$ and nucleation is eased since the overall surface energy required is less than for homogeneous nucleation. The nucleation rate given in Equation (2.10) is, after correcting for $\gamma_{het} < \gamma_{hom}$, also valid for 3D-heterogeneous nucleation (Mullin, 2001).

2D-heterogeneous nucleation is restricted to growth in z-direction, resulting in a disk-shaped crystal, as illustrated in Figure 4b. The nucleation rate is given as

$$J = B\exp\left(-\frac{\pi\kappa\gamma^2 v}{k^2 T^2 \ln S}\right)$$

(2.12)

where B is a pre-exponential kinetic parameter representing the attachment frequency of monomers to the nucleus and κ the thickness of the 2D-nucleus. The difference between 2D- and 3D-nucleation in terms of energy is equal to $\frac{16\gamma v}{3\kappa kT\ln S}$. A high degree of local supersaturation is required for 2D-nucleation to occur. Still, the energy barrier is lower for formation of 2D-nuclei than 3D-nuclei (Mullin, 2001).

Although scale deposition on surfaces is considered to be mainly heterogeneous (Chen et al., 2005), the presence of solute crystals can induce the formation of new crystals and thus, secondary nucleation.

2.4.3 Induction time

The induction time is the time from achieving supersaturation to the appearance if (detectable) crystals and consists of three parts; the relaxation time to achieve quasi-steady-state distributions of molecular clusters, the nucleation time and the latent period. The latent period corresponds to the time it takes before onset of a detectable change occurs. The three periods are illustrated in Figure 5 below.

 Induction time is impacted by level of supersaturation, agitation, foreign particles and viscosity. It is easiest illustrated by a desupersaturation curve as seen in batch experiments, see Figure 5. The region of growth corresponds to the decrease in concentration from solution. For a continuous system where reactants are continuously supplied, this decrease in concentration would not be seen.
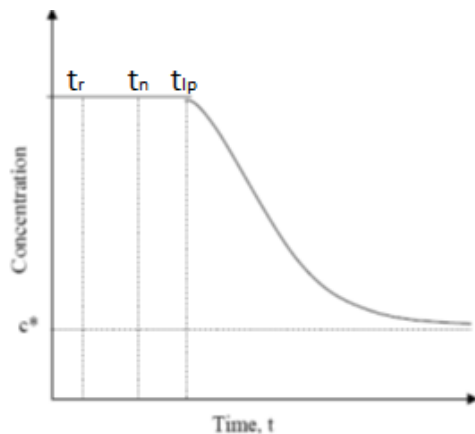

Figure 5: Desupersaturation curve for a batch experiment; t_r=relaxation time, t_n=nucleation time and t_{lp}=latent period

2.5 Crystal growth

After stable nuclei have formed, the nuclei will enlarge themselves into particles of detectable size. There exist several theories to explain how this growth happens, of which the adsorption layer theory and the diffusion-reaction theory can be mentioned as examples (Mullin, 2001). Each of these will be discussed further on.

In general, a characteristic dimension of the growing particle can be identified. The linear growth rate can be defined as

10

$$G = \frac{dL}{dt} \tag{2.13}$$

where L is the chosen characteristic length.

2.5.1 Growth models

Volmer postulated a mechanism of crystal growth based on an adsorbed layer of solute atoms on a crystal face. Solute atoms arriving at a crystalline substance will migrate freely over the crystal surface and link themselves into the lattice at active centers; i.e. where the attractive forces are strongest. This scheme repeats until one layer of the crystal face is complete. Before further growth can happen, a new "centre of crystallization" must be created, thus, only one layer grows at a time (Mullin, 2001).

Another model based on mass transfer concepts were suggested by, among others, Berthoud and Valeton. This model has two steps; mass transfer (diffusion) of molecules or ions from the bulk solution to the surface and the subsequent surface integration ("reaction" with the surface into the lattice) takes place. Hence, the name diffusion-reaction is often used. The principle is illustrated in Figure 6 below.
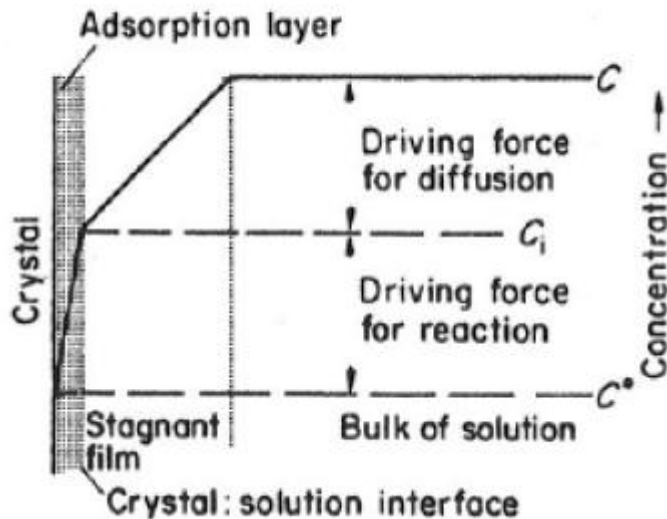

Figure 6: Diffusion - reaction model; the driving force for diffusion is the concentration difference between the bulk concentration, C, and the interface concentration, Ci. The driving force for reaction is the difference between Ci and the equilibrium concentration C* at the crystal surface.

Either of the two steps (diffusion and reaction) can be rate determining: If crystallization takes place at a surface where a significant boundary layer exist (which can be the case where flowing solution meet a stagnant surface), mass transfer may be the limiting step. Conversely, if crystals are formed in the bulk solution and transported as solids towards the surface, the reaction step can be rate determining.

By combining the mass transfer expressions for the diffusion and the reaction steps, an overall growth rate order can be obtained

$$G = \frac{dm}{dt} = AK_g \left(c - c^* \right)^g$$

(2.14)

where A is the area of the crystal receiving the deposit, K_g an overall crystal growth coefficient and g the growth order. An assumption for this equation is that the deposition rate at the crystal surface is proportional to the concentration difference between the deposition point and the bulk solution.

2.5.2 Growth of sparingly soluble electrolytes

For sparingly soluble electrolytes it is suggested that reaction kinetics are rate determining. As cited by Cowan and Weintritt (1976), Doremus studied precipitation of sparingly soluble electrolytes from solution. He concluded that the order of the crystallization process depend highly upon the stoichiometry of the electrolyte and its supersaturation. Nancollas (1983) (as cited by Bott (1995)) argues that the rate of crystallization at the surface is to a small degree impacted by changes in fluid dynamics, hence, another mechanism than diffusion is controlling. In addition, activation energies for crystal growth are usually considered to be higher than activation energies for bulk diffusion. Based on this, Nancollas suggested the following rate expression for a salt with generalized formula $M_a X_b$:

$$G = \frac{d(M_a X_b)}{dt} = -k_r S K_{sp}^{\frac{g}{v}} \sigma^g$$

(2.15)

in which k_r is the rate constant, S an function of the surface area, g the growth order, $v = a + b$ and

$$\sigma = \left[(M^{m+})^a (X^{x-})^b \right]^{\frac{1}{v}} - K_{sp}^{\frac{1}{v}}$$

(2.16)

Using activities for the lattice ions and lumping k_r and S together, Equations (2.15) and (2.16) can be combined to yield the following relation for crystal growth controlled by surface integration:

$$G = k_g \left(S - 1 \right)^g$$

(2.17)

where S is the supersaturation as defined in Equation (2.7), k_g is the lumped growth rate constant and g the growth order.

The growth rate constant can be expressed in an Arrhenius form as

$$k_g = Ae^{\frac{-E}{RT}}$$

Here, A is a constant, E the activation energy, R the universal gas constant and T the temperature.

2.5.3 Correlation between growth order, growth mechanism and morphology

Growth controlled by the surface reaction is a discrete step-by-step process. For growth to occur, a step or kink must be formed. Thereafter, integration into the lattice will take place at such active centers where the attractive forces are greatest. Different mechanisms can be distinguished based on whether it is nucleation at the surface or lattice defects that form these active centers. Nucleation at the surface can also be further differentiated in layered growth, where one complete layer builds on another, and birth-and-spread, where nuclei are formed at the same time as lateral growth take place (Mullin, 2001).

Examples of these three mechanisms are shown in Figure 7 below. As the active centers are formed, growth will be the result of a sequence of steps such as; mass transfer of reactants to the surface (diffusion), adsorption at the surface, diffusion at the surface, surface reaction and integration into the crystal lattice (Mullin, 2001).
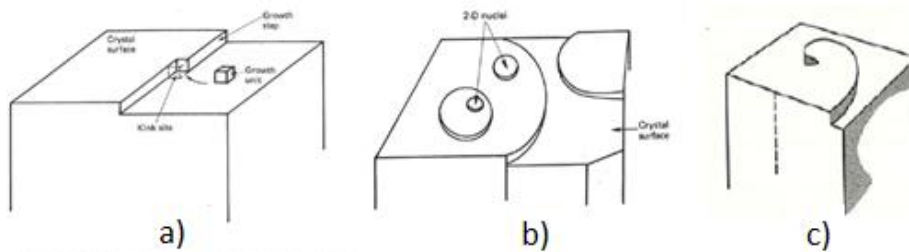

Figure 7: Growth models; a) layer growth, b) surface nucleation, c) spiral growth at lattice defects

The growth order presented in Equation (2.17) can take different values depending on growth mechanism. When crystal growth is controlled by the diffusion of molecules or ions towards the surface rather than the integration into the lattice, only the concentration difference is of interest and g=1.

For growth rates controlled by surface reactions, three cases are possible: g=1, g=2 and g>2. Spiral growth will have g=2 and g=1 at respectively low and high supersaturations. The lower growth rate at high supersaturations can be explained by increased resistance in the film close to the surface; the film gets crowded by all the reactants and hence, the diffusion through the film is slower. That g=2 for even very low supersaturations, is explained by the screw dislocations, resulting in a never-smooth surface promoting growth.

When the supersaturation is high, polynuclear growth can occur at the surface. Nucleation generates the necessary steps, so that lateral growth can take place at the same time as other nuclei are formed. This can give g>2. The rate of nucleation versus the rate of lateral growth determines whether the surface will be smooth or rough. At high supersaturations, the nucleation rate dominates and gives a rough surface. In this case, g=1, since surface integration will almost occur immediately and mass transfer of reactants will be the rate determining step(Andreassen, 2010).
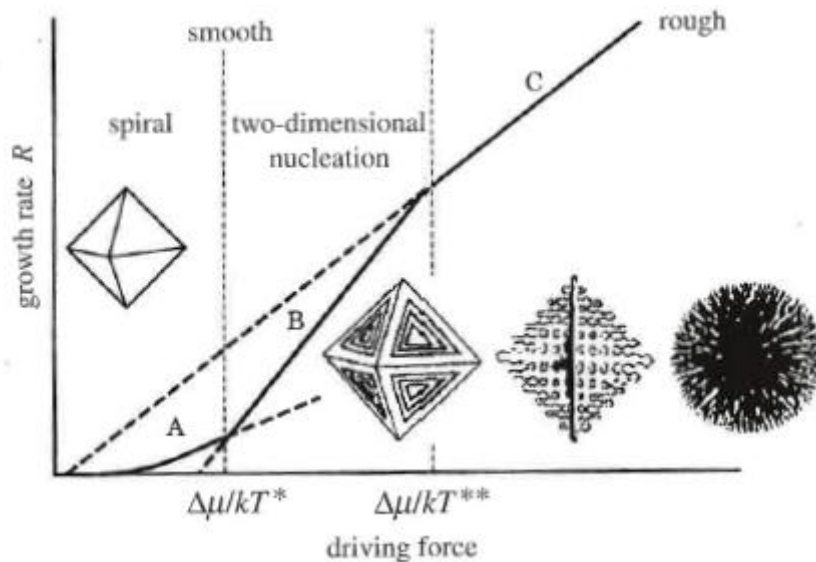

Figure 8: Changes in morphology in relation to growth rate and supersaturation (driving force) (Sunagawa, 2005)

In Figure 8, growth rate as a function of supersaturation is coupled with the different growth mechanisms and morphology. As the three different mechanisms have different growth orders, the curve will change in shape with increasing supersaturation. In regime A, the interface is smooth and growth is primarily controlled by spiral growth. In the first bending point, regime B starts. Here, two-dimensional nucleation will be the dominating mechanism, but the surface is still smooth. As the interface becomes rough in regime C, diffusion will control the crystal growth. This creates crystals without flat faces; spheres or dendrites.

2.5.4 Special growth mechanisms

If the crystallization occurs rapidly, tree-like formations called dendrites are often formed (Figure 9). The growth is controlled by diffusion. Hence, the parts of the crystals furthest into the supersaturated medium will experience the highest supersaturation. Thus, these parts grow more rapid. As supersaturation is consumed at the end of the growing crystal, local variations and areas with higher supersaturation can occur elsewhere. This causes branches to grow out of the stem into the supersaturated areas (Mullin, 2001).
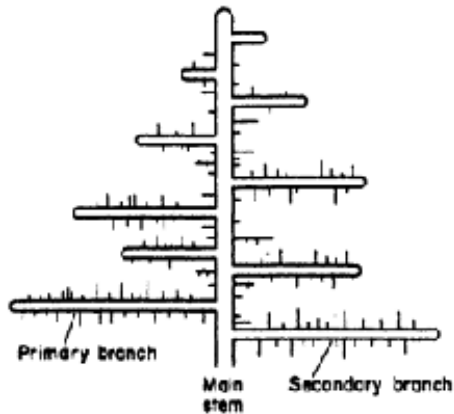
A special case of crystal growth is the formation of spherulites. The theories around spherulites are debated, so here, only the concept will be introduced. Gránásy et al.(2005) suggest that spherulitic particles have two different growth mechanisms, as illustrated in Figure 10 below. Type I-spherulites are a result of multidirectional growth from one central precursor. Formation of type II- spherulites start with a single crystal precursor, which via uniaxial growth and low angle branching end up as a fully developed spherulite.
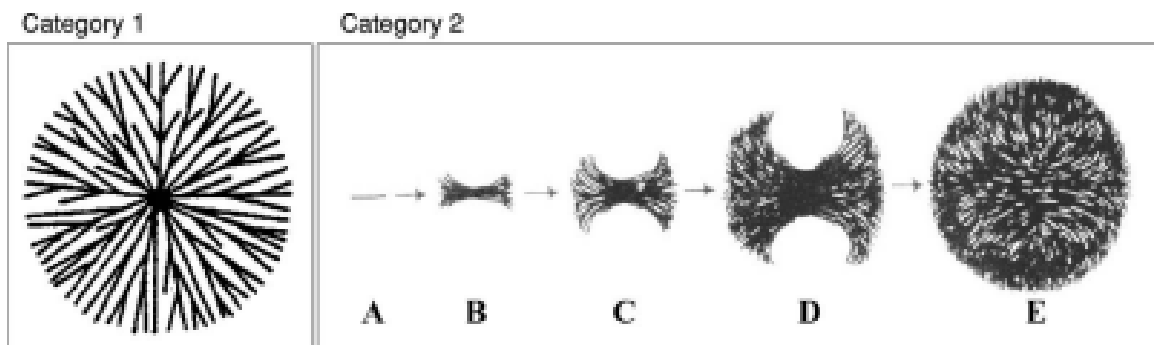

Figure 10: Type I (left) and type II (right) growth of spherulitic particles (Granasy et al., 2005)

2.6 The calcium carbonate-system

In an aqueous solution, calcium carbonate experiences the following main equilibriums:

$$CO_2(g) = CO_2(l) \tag{2.19}$$

$$CO_2(aq) + H_2O = H^+ + HCO_3^- \tag{2.20}$$

$$HCO_3^- = H^+ + CO_3^{2-} \tag{2.21}$$

$$Ca^{2+}(aq) + CO_3^{2-}(aq) = CaCO_3(s) \tag{2.22}$$

A complete list of equlibria and their equilibrium constants are given in Appendix F. The supersaturation ratio for calcium carbonate, as defined in Equation (2.7), can be written as

$$S = \left(\frac{a_{Ca^{2+}} \cdot a_{CO_3^{2-}}}{K_{sp}(CaCO_3)} \right)^{\frac{1}{2}} \tag{2.23}$$

pH is defined as the negative logarithm of the concentration of hydronium ions, H_3O^+, though, more commonly used is the concentration of protons, H^+-ions. As seen from Equation(2.4), by multiplying the concentration of H^+-ions by activity coefficient, a relationship between pH and activity can be established. From the equilibrium reactions given in Equations (2.19)-(2.22) follows that the carbonate activity is linked to the H^+-activity. Thus, as pH increases, so does the activity of carbonate. From Equation (2.23) it consequently follows that increased pH means increased supersaturation. Contrary; precipitation of calcium carbonate will decrease pH.
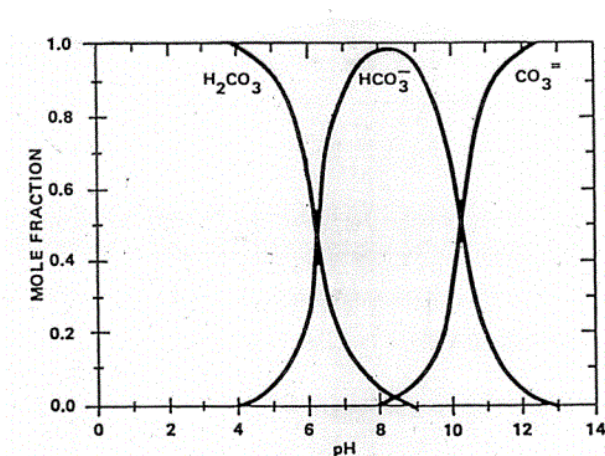

Figure 11: Bicarbonate - carbonate distribution as function of pH

Each of the carbonate products in Equations (2.19)-(2.21) has its preferred pH-region, as seen in Figure 10. When using sodium carbonate, Na_2CO_3, as carbonate source, a pH of about 10.4 is achieved. At this pH, about half the added carbonate will be present in the state of bicarbonate.

In order to determine which concentration of sodium carbonate that is required to maintain a given supersaturation, the systems alkalinity must be known. Alkalinity is a measure on a systems ability to resist a change in pH by neutralizing hydronium to the equivalent point of carbonate or bicarbonate. By setting up an electron balance for the sodium carbonate and calcium chloride system,

$$C_{Na^+} + 2C_{Ca^{2+}} + C_{H^+} = C_{HCO_3^-} + 2C_{CO_3^{2-}} + C_{OH^-} + C_{Cl^-}$$

(2.24)

species contributing to alkalinity can be identified. By ignoring weak acidic and basic species (as pH is high) and the dissociation product of neutral species, Equation (2.24) reduces to

$$C_{Na^+} = C_{HCO_3^-} + 2C_{CO_3^{2-}}$$

(2.25)

Hence, the alkalinity required to maintain a desired supersaturation ratio can be calculated based on the concentration of sodium ions. This is done in a simulation program such as MultiScale.

The solubility product of vaterite, calcite and aragonite are determined experimentally as (Plummer and Busenberg, 1982)

$$\log K_{sp,vaterite} = -172.1295 - 0.077993 \cdot T + \frac{3074.688}{T} + 71.595 \cdot \log T$$

(2.26)

$$\log K_{sp,aragonite} = -171.9773 - 0.077993 \cdot T + \frac{2903.293}{T} + 71.595 \cdot \log T$$

(2.27)

$$\log K_{sp,calcite} = -171.9065 - 0.077993 \cdot T + \frac{2839.319}{T} + 71.595 \cdot \log T$$

(2.28)

where T is the temperature in Kelvin. Using the solubility product from Equation (2.26)-(2.28), the supersaturation for the different polymorphs can be calculated through the relation

$$S_1 = S_2 \cdot \sqrt{\frac{K_2}{K_1}}$$

(2.29)

Calcium carbonate is an inverse soluble salt; meaning, its solubility product will decrease with increasing temperature. In contact with a heated surface, precipitation will occur due to

lower solubility at higher temperature. This is the opposite of most other ionic compounds. The inverse solubility is illustrated in Figure 12.
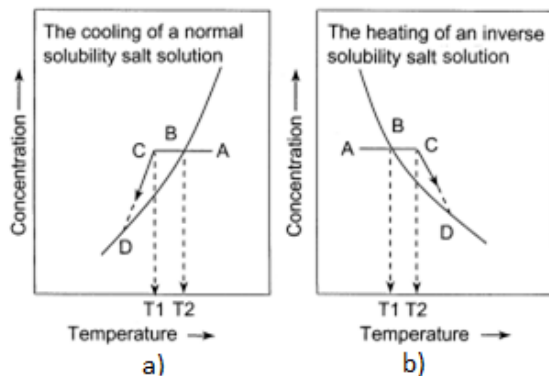

Figure 12: Solubility of a) a normal salt and b) an inverse soluble salt(Khan et al., 1996)

2.7 Polymorphism and morphology

A substance that can crystallize into chemically identical, but different crystallographic lattices, is named polymorph(s). The most stable polymorph has the lowest solubility, K_{sp}.

According to Ostwald's rule of stages the following stands; a crystallizing system will first crystallize out unstable phases, thereafter the more stable ones. The most stable phase is the one with the lowest free energy at a given temperature. This corresponds to the polymorph with the lowest solubility product. However, due to different kinetic and physical properties between different polymorphs, deviations from Ostwald's rule of stages are seen quite frequently. (Mullin, 2001)

 Different polymorphs cannot be separated on appearance only. Hence x-ray diffraction (XRD) patterns based on lattice parameters and the substance's crystallinity must be confronted in order to really distinguish between polymorphs.

2.7.1 Polymorphism of calcium carbonate

Calcium carbonate crystallizes in three different polymorphs; vaterite, aragonite and calcite, here listed by increasing stability. Vaterite has a polycrystalline, hexagonal structure. It has the highest solubility product and transforms easily to stable polymorphs. Aragonite has an orthorhombic structure and often forms needles. Calcite, the most stable polymorph, forms rhombohedral structures shaped like cubes (Flaten et al., 2009) . Both kinetics and thermodynamics contribute to the determination of the final composition of calcium carbonate. As seen in Figure 13, when the polymorphs precipitate from amorphous calcium carbonate, calcite dominates at lower temperatures and aragonite at higher. Vaterite is usually found at higher supersaturations.
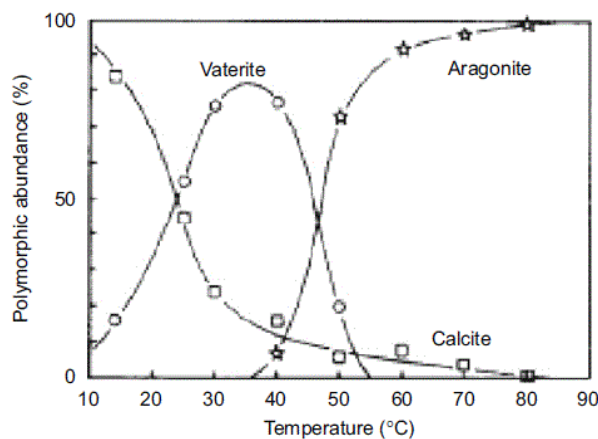
Figure 13: Temperature dependent polymorphic abundance (Ogino et al., 1987).

A slightly different distribution is found in the work by Kitano (1962) (as cited by Cowan and Weintritt (1976)). These data are obtained by precipitation from a calcium bicarbonate solution.
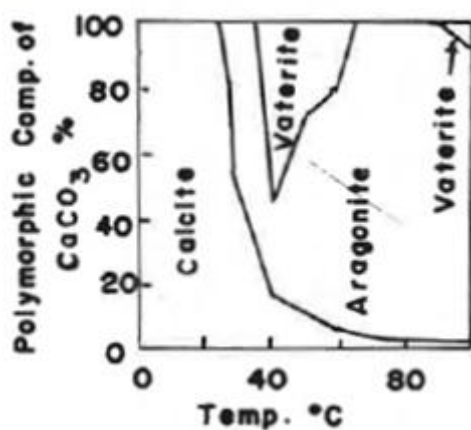
Figure 14: Percentwise polymorphic composition of calcium carbonate precipitated from a calcium chloride - bicarbonate solution(Cowan and Weintritt, 1976)

2.8 Formation and growth of scale

Scaling and fouling are closely connected, as discussed introductory in this chapter. Parts of the theory on scaling are based on general fouling theory, hence the common name crystallization fouling.

As described in Section 2.4, nucleation can be primary and secondary. Scale nucleation will take place at or close to the surface. If the scale nucleation takes place at the surface, sites such as kinks, edges and thermal spots can induce heterogeneous nucleation. Close to the

surface, presence of crystalline scale can induce secondary nucleation. Also, local supersaturations within the scale layer can lead to homogeneous nucleation.

Concentration and temperature profiles for a heat exchanger are illustrated in Figure 15. Here C is the bulk concentration, C_i the heat transfer/solution interface concentration and C^* the saturation concentration at the surface. Further, T_s is the temperature at the point of deposition and T_b the bulk liquid temperature. As for the case of general crystal growth, scaling in the heat exchanger can be controlled by diffusion, reaction or both (Bansal et al., 2008).
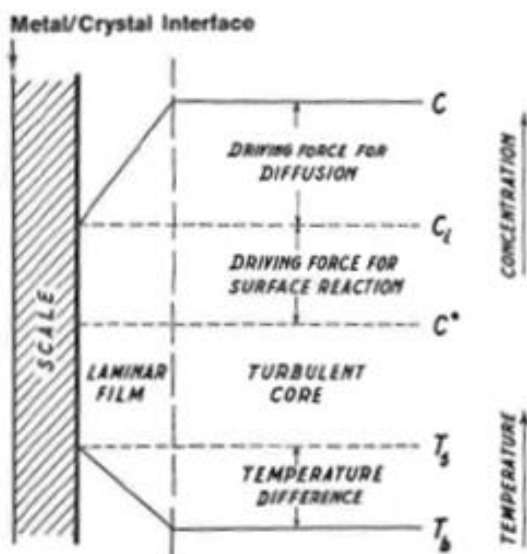
Figure 15: Driving forces for scaling on a heat exchanger (Cowan and Weintritt, 1976)

For fouling in general, it is observed that no deposition occur for some time at a new or cleaned heat exchanger. This period is referred to as the initiating period, conditioning period or induction period and is followed by a period of growth. (Bott, 1995), (Bansal et al., 2008). In Figure 16 below, a curve illustrating change in deposit thickness with time is given. Point A corresponds to the initiating period and B to a period of steady growth. C represents the region where the deposited layer remains virtually constant due to equal rates of formation and removal of depositions, either caused by weakly bound deposits or low mechanical strength in the deposited layer(Bansal et al., 2008).

Figure 16: Change in deposit thickness with time (Bott, 1995)

For a scaling system, removal rates can be neglected due to strong intermolecular bonds. On the other hand, the surface temperature will have a direct impact on the deposition thickness. As the scale thickness increases, the heat transferred from the heated surface underneath the solid layer will decrease. This gives a lower temperature at the surface in c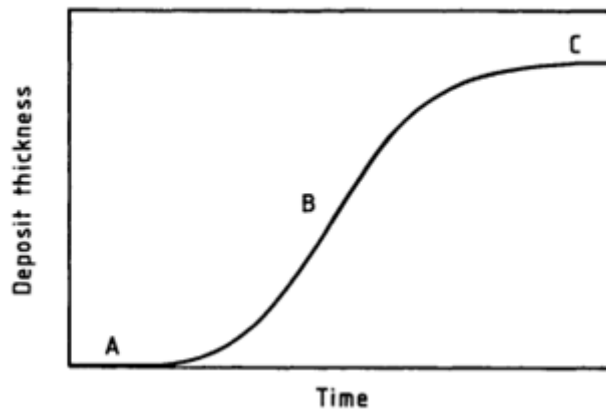ontact with the bulk solution and hence higher solubility and slower kinetics. Assuming that the scale growth rate will decrease when the scale layer reaches certain thickness is therefore not unreasonable.

Karabelas (2002) states that the factors responsible for scale formation in industrial processes can be classified into four categories; fluid composition, substrate surface properties, flow field (both in bulk and at the solid/liquid interface) and thermal field (heat flux, substrate surface temperature and bulk fluid temperature). This complexness also indicated that systematic studies should be performed to clearly separate the impact of the different factors on scale formation.

Scale growth can be inhibited by introducing a scale inhibitor. This inhibitor can hinder scale growth in several ways, where some of them are: Adsorption onto the face(s) of the scale nuclei to hinder further growth, blockage of active sites at the surface to prevent nucleation and growth or using a chelating agent which stoichiometrically blocks one of the reactants (for example calcium ions by adding EDTA). Also the presence of other ions and solvents can slow down or impact the scale growth in other ways (Crabtree et al., 1999).

2.9 Heat transfer

When a fluid outside a heated surface is in forced or natural motion, the heat transfer is said to be convective. The rate of heat transfer from the solid to the fluid can be expressed by

$$q = hA\left(T_w - T_f\right)$$

(2.30)

Here, q is the heat-transfer rate, A the heat transfer area, h is the convective heat-transfer coefficient, T_w is the temperature of the solid surface and T_f the average temperature of fluid flowing by (Skogestad, 2003).

For heat transferred through a wall, the term conductive heat transfer is used. For a hollow cylinder where heat is transferred from a fluid at the inside of the cylinder, the conductive heat rate can be written as

$$q = k \frac{2\pi L}{\ln\left(\frac{r_o}{r_i}\right)} (T_i - T_o)$$

(2.31)

Here, q is again the heat-transfer rate, k is the thermal conductivity, L the length of the cylinder (tube), T the temperature and r the radius. The subscript i and o refers to the inner and outer diameter of the cylinder, respectively.

Convection and conduction can be combined to yield a total expression for the heat-transfer rate. The heat-transfer coefficient can then be combined to an overall coefficient U. This is often done for heat exchangers.

A simple heat exchanger is illustrated in Figure 17. The amount of transferred heat depends on the temperature differences between hot and cold side, the contact area and the heat transfer coefficient in the material and also on whether the flow is flowing countercurrent or concurrent.
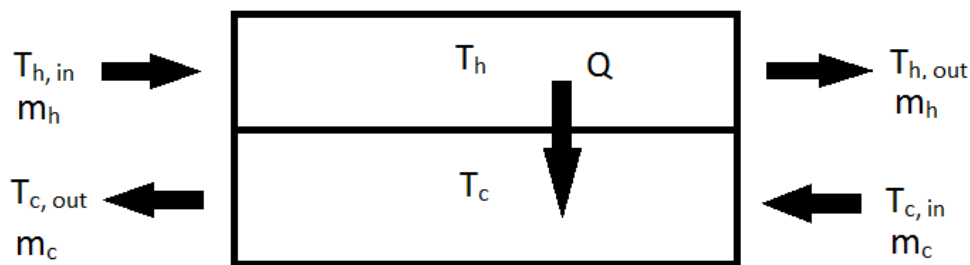
Figure 17: Principle sketch of a heat exchanger(Skogestad, 2003)

In the simplest case, the temperatures on each side are constant. For this case, the heat transfer can be described by

$$Q = UA\Delta T$$

(2.32)

Here, Q is the transferred heat, U the overall heat transfer coefficient, A the heat transfer area and ΔT the temperature difference between warm and cold side ($T_h - T_c$). In order to increase the amount of heat transferred, the area should be as large as (economically)

possible. One possible solution to this is to use a large number of narrow tubes. However, this type of arrangement has higher potential for scale blockage, since the diameter is so small. The amount of heat transferred can, for an ideal system at steady state, also be expressed by

$$Q = m_c c_{p,c}\left(T_{c,out} - T_{c,in}\right) = m_h c_{p,h}\left(T_{h,in} - T_{h,out}\right)$$

(2.33)

where m is the mass flow and c_p is the heat capacity of the fluid (Skogestad, 2003).

2.10 Continuous-stirred tank reactor

A continuous-stirred tank reactor (CSTR) is the most common continuous ideal reactor for liquid phase reactions, but the model works for all fluids. The reactor is assumed to be operated at steady state and to be perfectly mixed. Perfectly mixed refers to no time or spatial variations inside the reactor, that is all variables are the same at every point inside the reactor. The outlet concentration and temperature is therefore the same as inside the reactor. A sketch of the CSTR is given in Figure 18.
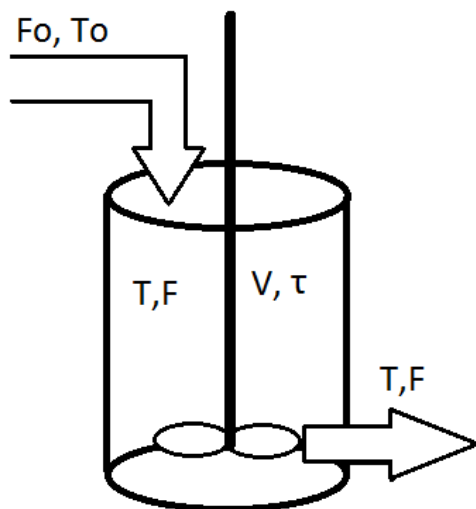
Figure 18: Schematic illustration of a CSTR

Residence time, defined below in Equation(2.34), is a commonly used parameter in chemical engineering. It is a measure of the time necessary to let one reactor volume of fluid, based on entrance conditions, enter the reactor. The residence time, τ, used is in reality the mean residence time and gives the average time a molecule spends in the reactor. Residence time is defined as

$$\tau \equiv \frac{V}{v_0}$$

(2.34)

Here, V is the volume and v_0 is the volumetric flow rate. The volumetric flow rate relates to the mass flow rate, F, and the concentration as $F = Cv_0$ (Fogler, 2005).

In stirred tanks, baffles are often placed, either on or off the wall, to modify the flow and destroy vortices. The most common is to have baffles on wall. However, such baffles can create dead zones in where the liquid more rarely is exchanged, as seen in Figure 19.
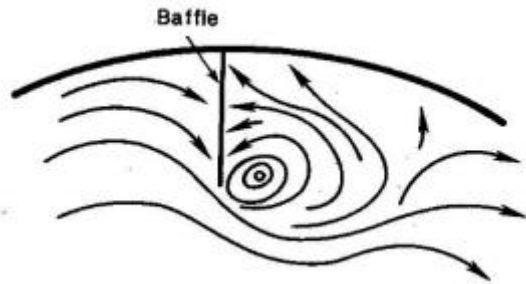
Figure 19: Vortice in tank with baffles on wall (Jakobsen, 2008)

2.11 Analysis techniques

2.11.1   Scanning Electron Microscope

A scanning electron microscope (SEM) creates an image of the sample surface by scanning it with an electron beam. Electrons interact with the atoms in the sample, producing signals containing information about the surface's topography and composition. One drawback with the SEM is its requirement for conducting samples, as charge of electrons else can build up. A solution is to coat the samples with a conductive material, but this can hide small topographic details (Tolchard, 2010).

SEM-pictures can be obtained detecting different kinds of electrons. Secondary electrons (SE) are reflected from the matter close to the surface. Such pictures will give more surface information, but are more sensitive to charging. Back scattering electrons (BSE) are reflected from further inside the sample. As heavier elements have more electrons, more electrons will be reflected from such. Hence, BSE creates a mass contrast between the elements in the sample, where the heavier elements will appear as brighter. An example of this is given in Figure 20, where the bright parts are the stainless steel surface and the darker parts calcium carbonate (Cao and Wang, 2011).

Figure 20: Image obtained by detection of backscattering electrons (left) and secondary electrons (right).

2.11.2 Powder X-ray diffraction

Powder X-ray diffraction (XRD) is used to characterize a powdered solid sample of a (poly) crystalline material. X-rays will be diffrac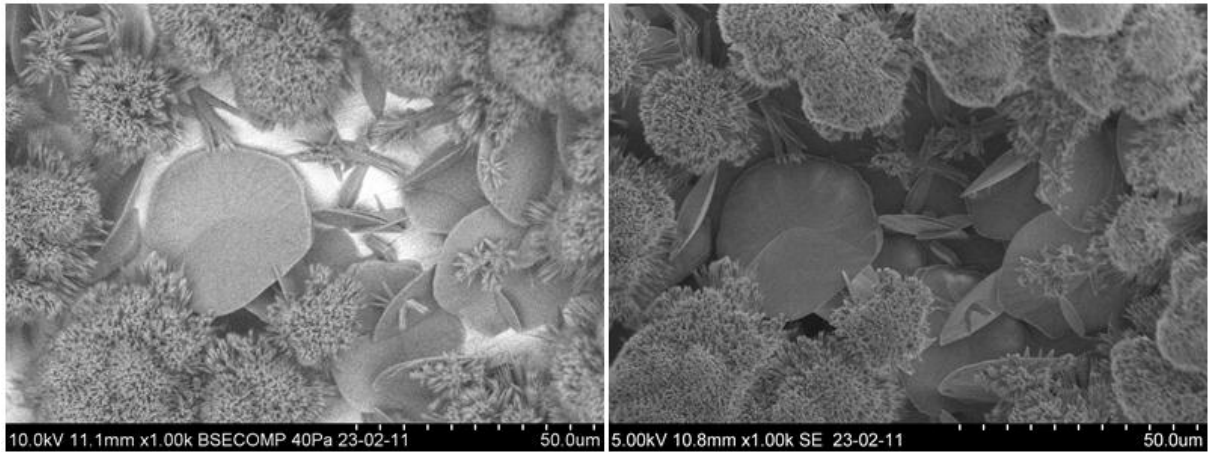ted by the crystalline matter and result in a pattern with intensity peaks at given positions for a given compound. These positions are usually referred to as 2θ-values, where θ is the Bragg angle. By looking at the position and shape of these peaks, information about the crystalline matter can be found (Callister, 2007).

Different polymorphs will have different diffractive patterns due to different crystalline lattice arrangements. Thus, the intensity of the characteristic peaks will increase with increasing degree of crystallinity of the given polymorph. For calcium carbonate, this means that calcite, with a high degree of crystallinity, often has more intensive peaks than the other polymorphs. This makes quantification of calcium carbonate somewhat more complex.

Different techniques are used for quantifying the amount of polymorphs from an XRD-pattern. One common method is to calculate the polymorphic ratio of the polymorphs from the integrated intensities of the XRD-spectra. Here, a calibration curve made from mixtures with known polymorphic ratio is required to correct for different degree of crystallinity in the different phases (Yang et al., 2002), (Flaten et al., 2009).

Another method is the Rietveld refinement method. This method is refining a theoretical line to match a measured X-ray spectrum by using the least squares method. Thereafter, integration is performed on this theoretical line. An assumption (which to some extent can be corrected for) is that the convolution of the effects contributing to the shape of the reflection (peak) has a Gaussian reflection (Rietveld, 1969). An important parameter in Rietvelt refinement is the structure factor, which is describing mathematically how a solid material will scatter incident radiation. This scattering originates from the periodic arrangement of the crystalline matter, as a distinct pattern of constructive and destructive

interferences is created when radiation interferes with the atoms in the unit cell (Elliott, 1998).

3 Experimental

A total of 51 experiments were conducted, all executed in the same experimental setup using the same procedure.

3.1 Apparatus

As stated introductorily, this experimental setup was designed with the purpose of studying scale formation on a heated surface as a continuous process. To comply with this, reactants were allowed to constantly pass by a heated surface. This surface was inserted into a stirred tank, in where the reactants experienced a certain residence time. A sketch of the experimental setup is given in Figure 21 below.

Reactor setup
A Reactor (stainless steel, unknown grade) with four fixed baffles
B Reactant supply tube
C U-shaped heated tube (SS316)
D Propeller
E pH-meter probe (InLab Expert connected to Metler Toledo SevenEasy pH-meter)
F Thermometer (VWR Traceable)
G Digital stirrer engine
I Calcium chloride supply
J Sodium carbonate supply
K Cooling jacket
L Thermostate (Lauda RE205)
M Thermostate (Julabo FP30)
N Excess liquid drain
O Reactant mixer
P Peristaltic pump (Masterflex easyload)
Temperature adjuster (two identical setups)
Q Temperature adjuster vessel
R Reactant inlet tube
S Reactant outlet tube
T Propeller
U Thermometer (VWR EU-630)
W Cooling/heating jacket
X Thermostate (Lauda RE205)
Y Peristaltic pump (Masterflex easyload)
Z Reactant reservoir

Figure 21: Experimental setup

Solutions of calcium chloride and sodium carbonate were pumped separately from their respective reservoirs by pump A, to two water-jacketed agitated vessels. These vessels served as temperature pre-adjusters, as it was experienced that the water jacket surrounding the reactor was not efficient enough. From the temperature adjuster vessels, the reactant solutions were pumped separately towards the reactor by pump B. Before entering the reactor, the reactants were mixed in a Y-tube. The outlet of this tube was placed under the reactor liquid surface, close to the reactor bottom. As excess liquid was transferred continuously from the reactor to a waste tank, the reactor held a constant volume of 2.0L.

Inside the reactor, a U-shaped water heated tube was inserted. The reactor was agitated by a four bladed down-pushing propeller connected to a mechanical agitator. A thermometer monitored the temperature of the bulk liquid. To indicate changes in the bulk liquid composition, a pH electrode was introduced to the reactor. This instrument did also contain a temperature probe, which was in accordance with the thermometer.

The relative placement of the different reactor equipment is illustrated in Figure 22 below. Some of the placements were dictated by the fixed positions of the reactor outlet, propeller radius and the baffles.

1 Propeller and corresponding required radius
2 Reactant supply tube
3 pH-meter
4 Thermometer
5 Heated tube
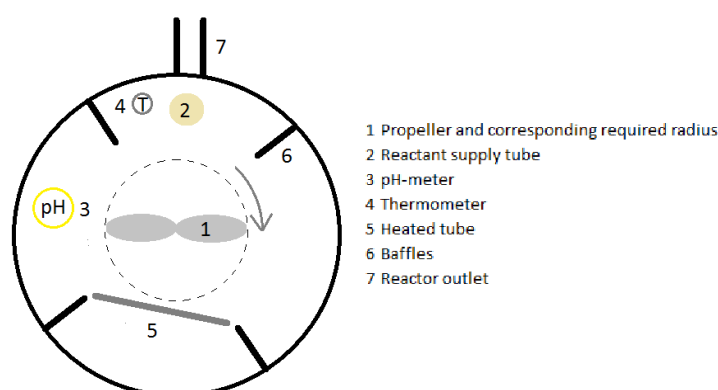6 Baffles
7 Reactor outlet

Figure 22: Relative placement of equipment in reactor

Agitator, pumps and thermostats were assigned set points as listed in Table 1 below. These parameters were constant throughout the experiment, although slight fluctuations were observed (as listed). The relative large variation in pump capacity is explained in Appendix B. Set points for the thermostats were given to match the desired experimental conditions: first, the tube temperature was set. Thereafter, the jacket temperatures were adjusted until the desired bulk temperature was complied. These jacket temperatures were then used as set points for the jacket thermostats.

Table 1: Fixed apparatus parameters

Device	Unit	Value
Agitators	Rpm	1000±10
Peristaltic pumps	g/min	670±60
Julabo thermostat (heated tube)	°C	Setpoint±2.0
Lauda thermostats (jackets)	°C	Setpoint±0.5
Reactant reservoir container	kg	28.0±0.15

An example of the tube used as heated surface is shown in Figure 23. A list of all the tubes with surface areas are given in Appendix E.

Figure 23: U-shaped tube. When heated internally by water, a heated surface is created

3.2 Supersaturation

In all experiments conducted, supersaturation is an important parameter. As stated, supersaturation will change with temperature and the amount of ions in the solution. In this work, a reference to a given supersaturation corresponds to the supersaturation of calcite calculated from the initial reactant concentrations and the reactor bulk liquid temperature. In reality, the actual supersaturation inside the reactor will be lower due to two factors: the amount of ions in solution will be lower than the initial level as supersaturation is consumed by precipitation. In addition, the heated surface changes the temperature in the boundary layer and thus, the supersaturation. It should also be noted that the supersaturation of other polymorphs will be lower than what it is for calcite. Further details on this can be found in Appendix F.

3.3 Experimental conditions

The experiments were divided into two main groups: first some initial tests were performed before the main focus was directed to experiments on scale growth rate determination.

In the first set, different apparatus settings was tested to declare parameters for following experiments. Also the degree of scale coverage at the surface was studied. The matrix of experimental conditions is listed in Table 2 below and is read as follow: At constant

supersaturation, tube- and bulk temperature, three different agitation speeds were tested against two different reactant introduction methods, giving a total of six experiments.

Table 2: Initial experiments

S	T_{tube}(°C)	T_{bulk} (°C)	Agitation (rpm)			Introduction of reactants
6	90	30	0	500	1000	Separate
						Mixed in a Y-tube

As stated in Section 2.5, crystal growth rate is a function of both as supersaturation and temperature. In order to separate the effects of these parameters, only one of these parameters was varied at a time. Both tube temperature and bulk temperature was varied. Also, the experiment length was varied. This was done by preparing more than one batch (containers with 28 kg mixed solution) of reactants and introducing them successive so the flow was kept continuous. For all scale growth rate experiments, agitation was 1000 rpm and reactants were mixed in a Y-tube before entering the reactor.

In Table 3 below, the experimental permutations on scale growth rate experiments are summarized. The experiments are classified into five groups based on what they are investigating. Each combination is read in the same way as the matrix in Table 2.

Table 3: Scale growth rate experiments

T_{tube} [°C]			T_{bulk} [°C]			Supersaturation (S)								Experiment length [min]			
90			70	50	30	6								180			
90	70	50	30			6								90	180[2]	270	360[3]
90			30			4	4.5	5	6	8	10	12	20	90		180[1]	
90			30			20								45	90	135	180
90			30			6								90	180	270	360

[1] only performed for S=4 and S=8, [2] not performed for T_{tube}=50°C,

[3] not performed for T_{tube}=50°C and T_{tube}=70°C

3.4 Experimental procedure

Reactant solutions were prepared batchwise by dissolving calcium chloride dihydrate and sodium carbonate in equal weights of distilled water (28.0 kg). Before starting the experiment, all thermostats were at the given set point temperature. Agitators were turned on. The reactor was filled with distilled water. This water absorbed some of the heat from the heated tube, allowing the system to faster obtain steady state temperature after onset. The temperature adjustment vessels were filled with reactant solutions.

Pump B was set at speed value 9.0, corresponding to a flow of approximately $620\,\text{g/min}$, giving a residence time of 3.2 minutes. Each batch used approximately 90 minutes through the system. Pump A had a different speed scale and was set at the value giving the same flow as pump B.

Time was recorded with a stop watch from the start of the experiment, defined as when pump B was turned on. When one batch of reactants was emptied, this was immediately replaced to make the experiment run continuously. The experiment was run until one of the reactants was depleted. After finishing, the thermostats and agitators were turned off. Carefully, the scaled tube was elevated from the reactor and removed. When the tube was dry, it was weighed to determine the amount of scale.

Throughout the experiment, temperature and pH was monitored. Samples of the bulk fluid were withdrawn frequently with a 25 mL syringe. These were filtrated through Millipore 0.22µm attachable filter and analyzed by off-line titration for calcium content. For some experiments, a sample of the bulk fluid was collected from the reactor outlet for one minute. This sample was filtrated through a 47mm Durapore 0.22µm filter using a vacuum pump. About 25mL ethanol was used to wash the filtered crystals before the filter was dried and the crystals investigated by SEM.

After the experiment, the reactor vessel was emptied. As illustrated in Figure 24, scale was deposited in the reactor; the amount increasing with experiment length and supersaturation. The reactor was therefore thoroughly rinsed by the following procedure: A mixture of tap water and approximately 50 mL of 37wt% hydrochloric acid was stirred for five minutes in order to remove scale depositions. The reactor was emptied and rinsed with tap water. Then, the reactor was filled with 1mmol/kg solution of sodium carbonate to neutralize the acid. After five minutes, the reactor was emptied and rinsed well with tap water. Last, the reactor was rinsed with distilled water, emptied and allowed to dry.

Figure 24: Scale depositions in reactor after completed experiment

Chemicals used in the experiment are listed in Table 8 in Appendix A.

3.5 Analysis

3.5.1 Experimental analysis

A pH meter was used to monitor the pH in the bulk solution during the experiment. When precipitation occurs, the pH will drop as a consequence of reduced alkalinity due to loss of carbonate. Constant pH after steady state is reached will indicate constant composition in the bulk liquid and thus, constant supersaturation.

Calcium titration with EDTA of the withdrawn bulk samples was performed by a Mettler Toledo DL53 titrator unit. The filtered sample was added distilled water to a total volume of 50 mL. To dissolve eventual precipitated calcium, about 5mL 10%hydrochloric acid were added. About 2-4mL ammonia/ammonium buffer solution were added afterwards to give a pH about 10. The titrator unit worked as follows: EDTA (0.001M) was added in discrete amounts to the sample. EDTA binds stoichiometrically to calcium ions. Two electrodes detect the voltage in the solution. This voltage drops significantly at the titration end point where all calcium ions are bound and free EDTA available. From the amount of EDTA required to reach the titration end point and the weight of the initial sample, the calcium concentration was determined.

To determine the amount of scale formed on the metal pipe, the dry pipe was weighed before and after the experiment on a three digit Mettler Toledo XS 1003S scale.

3.5.2 Scale analysis

The deposited scale was analyzed by scanning electron microscope (SEM) and x-ray powder diffraction (XRD).

For SEM analysis, a Hitachi S-3400 N scanning electron microscope was utilized. For filter samples, a small piece of the filter was fastened to a metal stub by double sided carbon tape. An Edwards Sputter Coater S150B was used to coat the samples with gold. The scaled metal tube was fastened to a metal disk with carbon tape. Given that coating would destroy valuable topographic information, these samples were not coated. To eliminate charging, most uncoated samples were analyzed by back scattering electrons (BSE) in low-vacuum mode. Typical settings were pressure of 40 Pascal, voltage at either 10 or 15 kV, emission current of 40 mA and working distance about 9mm.

To obtain XRD-spectra of the deposited scale, a D8-Focus diffractometer was used. The scale was scraped off the tube. In a mortar, the scale was fully pulverized with a pestle. Ethanol was added until the powder was wetted. On a single crystal silicon sample holder, a drop of the crystal solution was placed using a pipette. After the ethanol had vaporized, the sample was analyzed. For quantification analysis of the polymorphic distribution, the samples were scanned with scanning angels from 20° to 85° using step size 0.01° and six seconds per step. Quantification on the XRD-spectra was performed by using the TOPAS software, which is based on the Rietveld refining method. Qualitative scans were done by scanning from 20° to 60° using step size 0.01 and two seconds per step.

Further details on the quantification analysis, see Appendix G.

4 Results and discussion

This work has been structured around two goals; to study the nature of the scaling layer and to determine scaling rates.

In the following sections, only the integer value of the supersaturation is given in the text. An exception is the discussion of onset of scale formation, where the first digit is included. A total of 51 experiments were performed. All raw data with accurate values are given in Appendix H.

The polymorphs indicated are confirmed by XRD, see Appendix G for details. When the term "agglomerate" is used, this refers to a collection of crystallites which outer appearance is one larger unit.

All presented pictures of crystals are obtained by SEM as described in Subsection 3.5.2. If nothing else is stated, the scale is examined at the heated tube and the pictures are taken from above, looking down at the scale.

All relevant calculations performed are given in Appendix D.

4.1 Initial tests

Small modifications were made to the apparatus constructed in the project work fall 2010. Hence, some initial tests were required before the systematic study listed in Table 3 could be performed.

4.1.1 Reactant addition

When constructing the reactor lid, this was done so that reactants could be added either separately in two tubes or pre-mixed in one tube. Some experiments were therefore conducted to determine whether the reactants should be introduced separately to the reactor or not. The following parameters were used: S=6, T_{tube}=90°C, T_{bulk}=30°C. The experiments were run for 90 minutes.

As seen in Figure 25, there is no significant difference between the two alternatives. Particle size, scale amounts and the polymorphs present are all comparable. Somewhat more scale can be observed at 1000 rpm. Hence, premixing in a Y-mixer was chosen for further experiments.
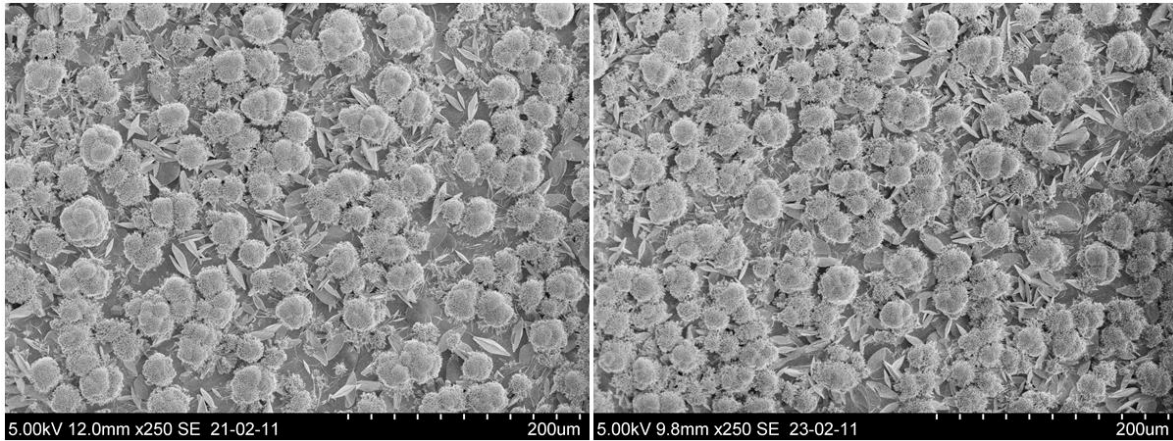
Figure 25: Appearance of crystals at separate addition (left) and premixing in Y (right) at 1000rpm. Scale bar is 200 μm.

4.1.2 Agitation

Reactor mixing is important for eliminating concentration gradients in order to be as close as possible to an ideal CSTR-reactor. Also, literature shows that the level of mixing affects the crystal nucleation to the extent that the critical supersaturation (onset of nucleation) decreases with increasing agitation (Mullin, 2001).

Two different impeller velocities and zero agitation were tested, with parameters as listed in Table 2. At higher velocities than 1000rpm, an upper constraint was found: aggressive mixing resulted in solution coming out through the lid openings.

In the experiment with no agitation, uneven distribution of scale was seen, in addition to scale growth due to bubble nucleation. From the SEM-pictures in Figure 26, it is evident that the degree of mixing impacts the amount of scale formed. Based on these results, 1000 rpm was set as standard impeller velocity.
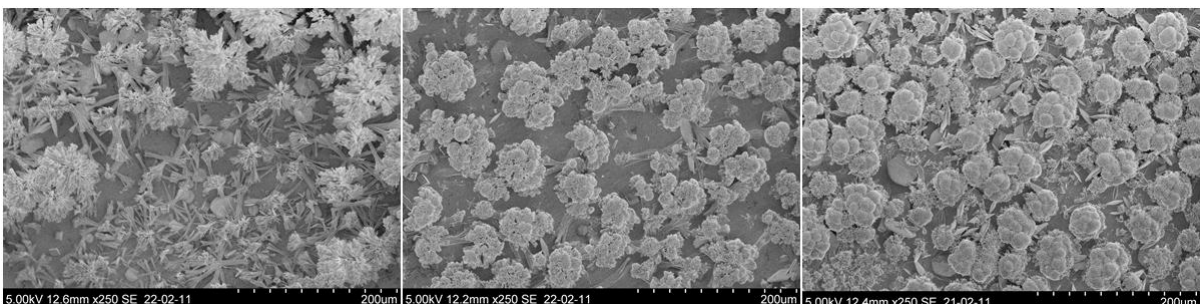

Figure 26: Appearance of crystals at agitation equal to 0 rpm (left), 500 rpm (middle) and 1000 rpm (rpm), reactants premixed in Y. The image scale bar is 200 μm.

In literature, continuous mixed tanks (CSTR) are rarely used to study scale formation. Most heat-exchangers are described by fluid dynamics where fluid velocity is an important parameter. High fluid velocity and turbulent flow generally implies thoroughly mixing. For scale formation of calcium carbonate, it was found in literature that increased fluid velocity

36

would decrease the induction period due to increased diffusion of ions towards the surface (Yang et al., 2002).

4.1.3 Surface coverage

Several authors point to scale growth as a two-step process, requiring an initial layer to be formed before successive growth takes place. This layer is formed in the initiating period, as discussed in Section 2.7. Rankin and Adamson (1973) reported on nucleation taking place at individual sites followed by lateral growth of these sites until the surface was completely covered. This was found both for isothermal systems and systems with heat transfer. Keysar et al. (1994) found that nucleation took place at localized sites at the surface during the initiation period. The initiation period is impacted by surface roughness, as deposits on a rough surface would adhere more easily than on a smooth surface. At higher supersaturations, the surface roughness increases, as discussed in relation to Figure 8. Higher supersaturation would therefore have a shorter initiation period.

Clarifying when the surface was fully covered would be important for the later growth rate experiments, which should be run long enough to pass the initial regime.
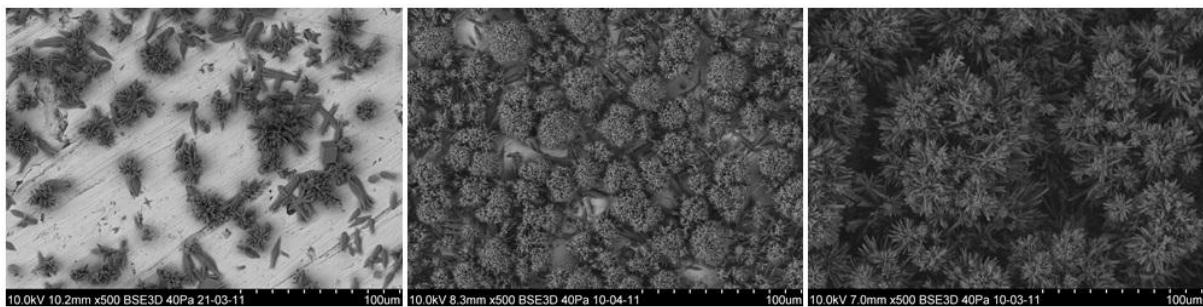

Figure 27: Scale after 45 minutes (left), 90 minutes (middle) and 180 minutes (right). The image scale bar is 100 µm.

Figure 27 illustrates that after 45 minutes, scale formation has started, but the surface is not completely covered. The scale formation is still in its initial phase. After 90 minutes, only minor unscaled spots can be seen between the scale conglomerates. At this duration, it is expected that the degree of surface coverage to some extent will vary to some extent from experiment to experiment. When the experiment has elapsed for 180 minutes, the surface is completely covered and the scale grows in layers.

On the basis of these results, growth rate experiments at S=6 should be conducted for minimum 90 minutes. For higher supersaturations, shorter experiment length can be used as the initiation period is expected to decrease.

4.1.4 Constant level of supersaturation

The project from fall 2010 indicated that the experiment, after reaching steady state at 30°C, would a have constant level of supersaturation. After changing some of the experimental parameters (agitation), this assumption should again be verified.
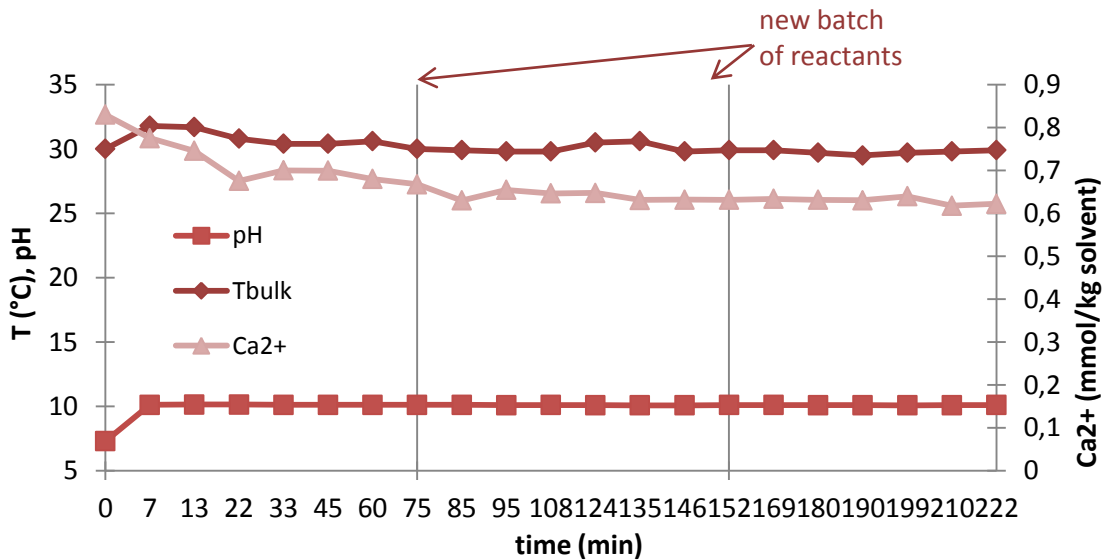

Figure 28: Temperature, pH and calcium concentration in the reactor bulk liquid (S=6, T_{tube}=90°C)

The bulk liquid temperature was expected to reach steady state quickly after the continuous flow of reactants started, as the reactant reservoirs were at room temperature and the thermostats at set points. From Figure 28 it is seen that the temperature deviates with less than 2°C throughout the experiment. The temperature fluctuations can be explained by the level in the pre-cooler vessels, which could vary with some deciliters.

Calcium concentration drops from the initial mixed concentration to a steady level after approximately 20 minutes, corresponding to about 6 residence times. Thereafter, the level only fluctuates. A drop in calcium concentration indicates that reactants are disappearing from the bulk solution. It can therefore be assumed that the drop in concentration is due to formation of solids, either in the form of scale at the surface or particles in the bulk solution.
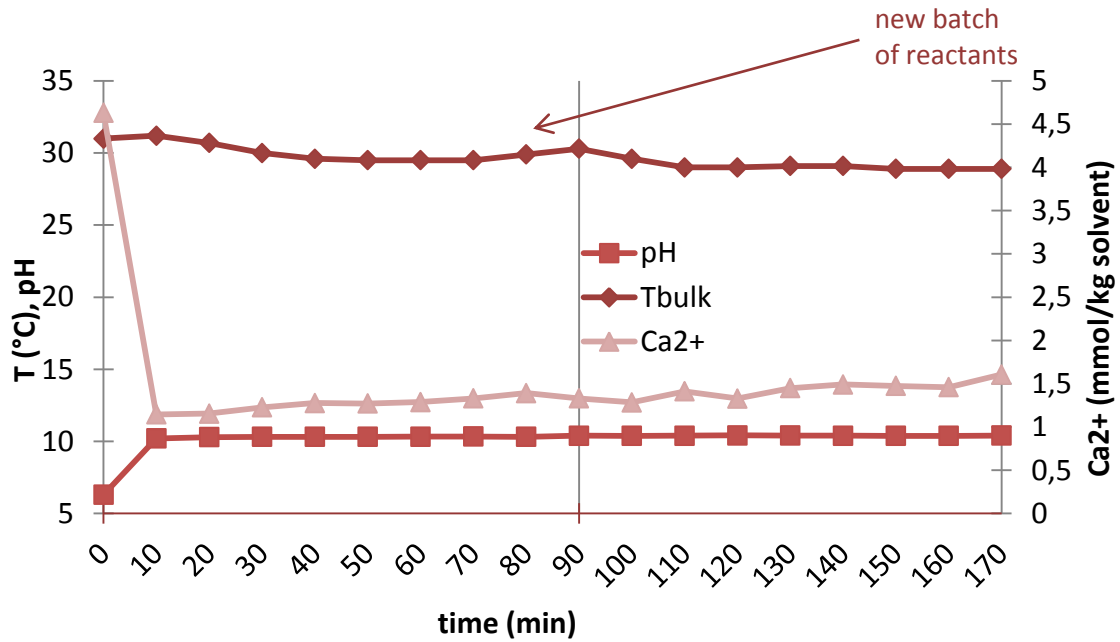
Figure 29: Temperature, pH and calcium concentration in the reactor bulk liquid (S=20, T_{tube}=90°C)

From Figure 28, it can be seen that similar trends of constant temperature, pH and calcium concentration are seen for S=20.

At constant temperature, a constant level of calcium ions can correspond to constant calcium activity, given that the other ions present in the solution are also at constant levels. In the experiments described here, the only species present are calcium chloride and sodium carbonate. The sodium level can be controlled indirectly by pH, as carbonate originating from sodium carbonate is the only pH-contributing specie. Before starting the experiment, the reactor vessel was filled with distilled water. As soon as the water was replaced by the reactant mixture, the pH was constant.

Based on the constant calcium concentration, the constant pH and the constant temperature, also the activity of ions in the reactor solution is presumed to be constant. Given these assumptions and the definition of supersaturation in Equation(2.3), the supersaturation can be said to be constant.

Introductory, heat exchange as a continuous process was discussed. In continuous systems, steady state will occur when the parameters are constant over time. An experimental setup where steady state is achieved allows for the study of scaling under more realistic conditions. Constant conditions, both over the whole area of scale formation and throughout the experiment, makes it is possible to tune the scaling parameters. This has not been demonstrated possible in setups where the scale formation is taking place inside a tube.

4.1.5 Initial supersaturation versus supersaturation at steady state

As mentioned, the steady state concentration of calcium shown in Figure 28 and Figure 29 differs from the initial concentration. In the reactor, the reactants will experience a thermal field from the heated tube, which impact the supersaturation. Also, supersaturation will be consumed due to precipitation of solids. The given initial supersaturation calculated based on the bulk temperature will therefore give a different degree of supersaturation than the effective supersaturation experienced close to the heated surface.

The steady state calcium concentration was determined by EDTA-titration. The concentration listed in Table 8 is the average concentration of the concentration profile shown in Figure 28 and Figure 29. Initial concentration is the concentration calculated from MultiScale, using the limiting reactant as basis.

Calcite, which has been used as the basis for supersaturation throughout this work, is the most stable polymorph. At equilibrium, it will therefore have he lowest activity and thus, higher supersaturation, see Equation(2.7). For aragonite, which is the dominant polymorph found in this work, the supersaturation is lower than for calcite. In Table 4, the initial and steady state supersaturations are calculated both with respect to calcite and to aragonite.

Table 4: Initial and steady state supersaturations for calcite and aragonite

Temperature [°C]	Initial			Steady state		
	Concentration of $CaCO_3$ [mmol/kg solvent]	Supersaturation		Concentration of $CaCO_3$ [mmol/kg solvent]	Supersaturation	
		Calcite	Aragonite		Calcite	Aragonite
30 (bulk)	0.83	6.2	5.3	0.66	4.6	3.9
90 (tube)		5.7	4.8		5.2	4.4
30 (bulk)	4.63	20.7	17.5	1.35	9.1	7.7
90 (tube)		20.0	16.9		8.5	7.2

As stated previousely, this work will use the term supersaturation on the initial supersaturation of calcite calculated from the bulk temperature, if nothing else is stated.

4.2 Effect of supersaturation

In Section 2.5, it was discussed how the solution composition and hence, the supersaturation, impacts the growth rate of crystalline matters. Two cases related to supersaturation was studied; the onset of scale formation was studied and one the relationship between supersaturation and mass deposited at the heated tube.

Both investigations were motivated by results from the project work performed fall 2010. Here, visual inspection (see Figure 30) indicated that the scale amounts increased from almost non-existing, to significant as the supersaturation was increased.
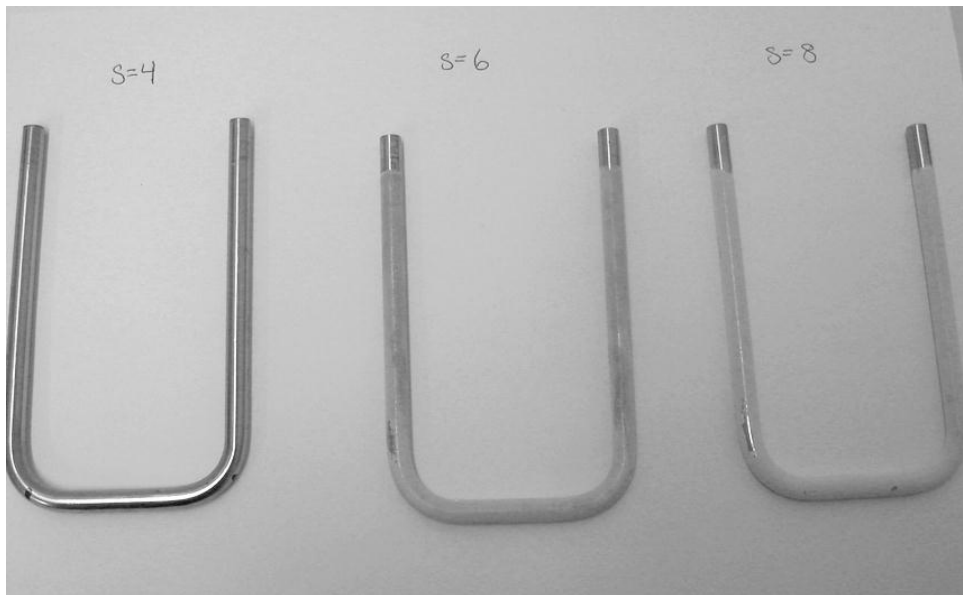

Figure 30: Increased scale formation with increasing supersaturation, fall 2010

4.2.1 Onset of scale formation

When introducing the driving force for crystallization in Subsection 2.3.1, it was stated that precipitation will occur in systems where S>1. As cited by Mullin (2001), Volmer specified that nucleation will occur in any supersaturated system, given sufficient time. However, the timescale can be millions of years (for a general system). A lower supersaturation where nucleation takes place within reasonable time, exists; the critical supersaturation.

Experiments with increasing supersaturation, T_{tube}=90°C and T_{bulk}=30°C were performed to investigate the critical supersaturation and corresponding onset of scale formation. The resulting SEM-images are presented in Figure 31.
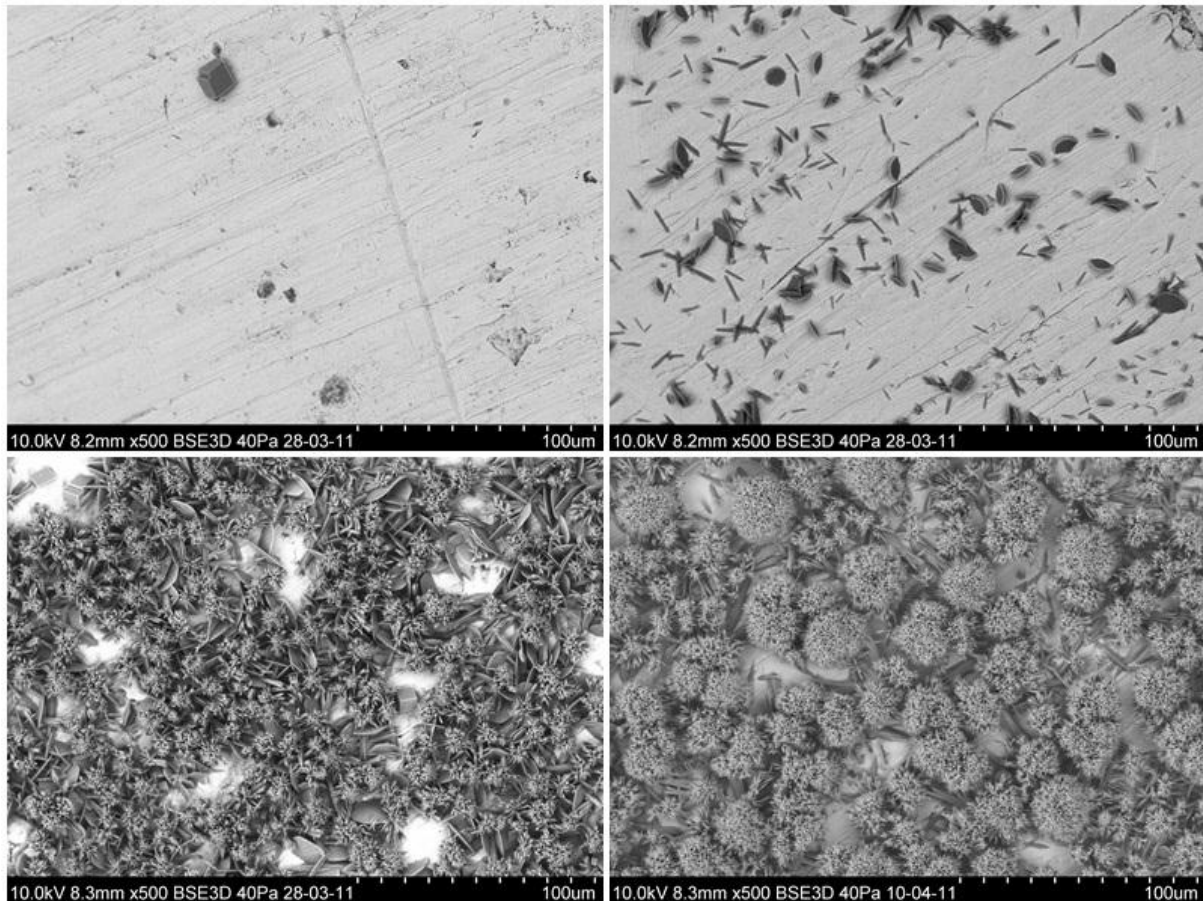
Figure 31: Scale formation for S=4.3 after 180 min (upper left), S=4.7 after 90 min (upper right), S=5.3 after 90 min (lower left) and S=6.3 after 90 min (lower right). The image scale bar is 100 μm.

At S=4.3, Figure 31 above reveals that only a few calcite crystals were formed after 180 minutes. By raising the supersaturation with 0.4, suddenly hundreds of crystals appeared in a comparable section, even though this experiment was run for half the time; 90 minutes. The crystals are mostly separate crystals of vaterite and aragonite, but also calcite can be seen. Raising the supersaturation even further, to S=5.3, resulted in a surface almost completely covered by scale. In this experiment, vaterite seemed to dominate at the surface, while aragonite was growing on top of the vaterite plates. As the supersaturation was raised to 6.3, only minor spots at the surface were without scale. Now, layered growth took place. Larger units of crystallites, agglomerates, of aragonite were observed on top of the initial layer.

The onset of precipitation at higher supersaturations than 1 can be described by slow kinetics, as pointed to by Volmer. Even though nucleation can occur at any S>1, the time for spontaneous nucleation will decrease with increasing supersaturation. Based on the experiments and the results in Figure 31, it appears as an onset of scale formation for this system exists around a critical value of S~4.5.

Cowan and Weintritt (1976) stated that the scale growth rate will, for a given supersaturation and contact time, be greater once the scale has formed than during

nucleation. They explained this by two different growth regimes. During initiation period, nucleation and growth occurred at the metal surface. When this surface was covered by a scale layer, growth took place at the already formed crystals of calcium carbonate. This is in accordance with the phenomenon described in Figure 16. In this study, the shift in mechanism from slow growth in the initiating phase to more rapid growth, can therefore be explain by the great difference in number of crystals be at S=4.3 and S=5.3.

Yang et.al (2002) has also observed calcite formation at surfaces where other polymorphs could be expected to precipitate. They also explain this by the two different scaling modes (A and B) described in Section 2.7. During the initiation period, the growth rate of calcium carbonate (as a general compound) will be lower. Slow rate favors formation of the most thermodynamically stable form. In the growth period, however, the general growth rate is higher, supporting formation the metastable, kinetically favored polymorphs. This highlights the complexness of crystal growth as both a thermodynamical and kinetic process.

The impact of different tube surfaces on the morphology is discussed in Appendix E.

4.2.2 Increasing supersaturation

Experiments with T_{tube}=90°C, T_{bulk}=30°C and experiment length 90 minutes were conducted for a range of supersaturations. The resulting SEM-pictures are given in Figure 32.

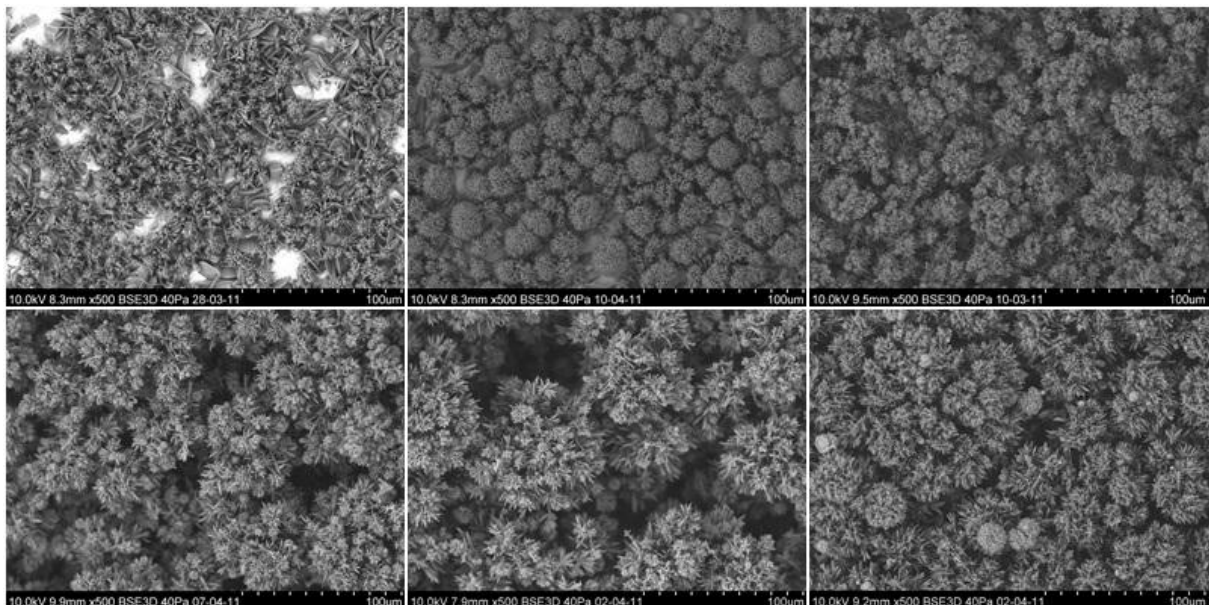Figure   32:   Upper   row: S=5(left),   S=6(middle),   S=8(right)
Lower row: (S=10 (left), S=12(middle), S=20(right). The image scale bar is 100 μm.

Figure 32 reveal how the amount of scale increases with increasing supersaturation. The scale layer grows outwards and the pictures show the top layer. Also, the morphology changes slightly with supersaturation.

At S=6, hemispheric agglomerates of aragonite needles (hedgehog-like) with sizes about 20 µm are growing on the initial surface layer. Smaller, less developed agglomerates exist in between the hemispherical ones. As the supersaturation increase to 8, the agglomerates get less defined; the hedgehog- structure is no longer visible. The agglomerates seem to consist of branched structures where type-I spherulites nucleate at the already formed needles in a dendritic-like pattern. The top layer is also less uniform and void spaces inwhere the surface still is visible, are seen between the agglomerates. This indicates that the crystalline structures are growing outwards on top on the initial agglomerates formed at the surface. Further, it points to a low degree of mixing into the inner layers and hence, insufficient supply of reactants to fill the void spaces. It can be speculated in whether the supply will ever be sufficient to fill these voids as reactants constantly are consumed by the outer layers. This can imply that such scale layers always will be quite porous, where the degree of porosity is determined by the growth rate and types of polymorphs formed. Literature states that rapidly deposited scale layers of calcium carbonate usually exhibits a porous structure (Cowan and Weintritt, 1976).

Raising supersaturation even more (from 10 to 20), the upper layers display more intricate topography. As a result of this topography, some areas at the surface are out of focus due to lack of depth of field. For the highest supersaturation studied, S=20, spherulites of both vaterite and aragonite are seen in between the branched structures. At high supersaturations, vaterite is not uncommon (Flaten et al., 2009). The spherulites are not attached to the branched structure, which indicates that they are nucleated from the more stagnant supersaturated solution between the branches.

Andritsos et al (1997) refers to two studies performed on scale of calcium carbonate on heat transfer surfaces. One study found that at bulk temperature 30°C and surface temperature 54-56°C, aragonite was the dominating polymorph. The other study concluded also on scales consisting primarily of aragonite. No further information on supersaturation or condition is given. However, it was pointed out that the aragonite crystals initially was shaped as needles, but changed with time to yield a dendritic 3D-structure.

For the experiments performed in this study, the mass gain was divided by the surface area of the tube available for scaling. In Figure 33, this mass gain is presented as a function of supersaturation.
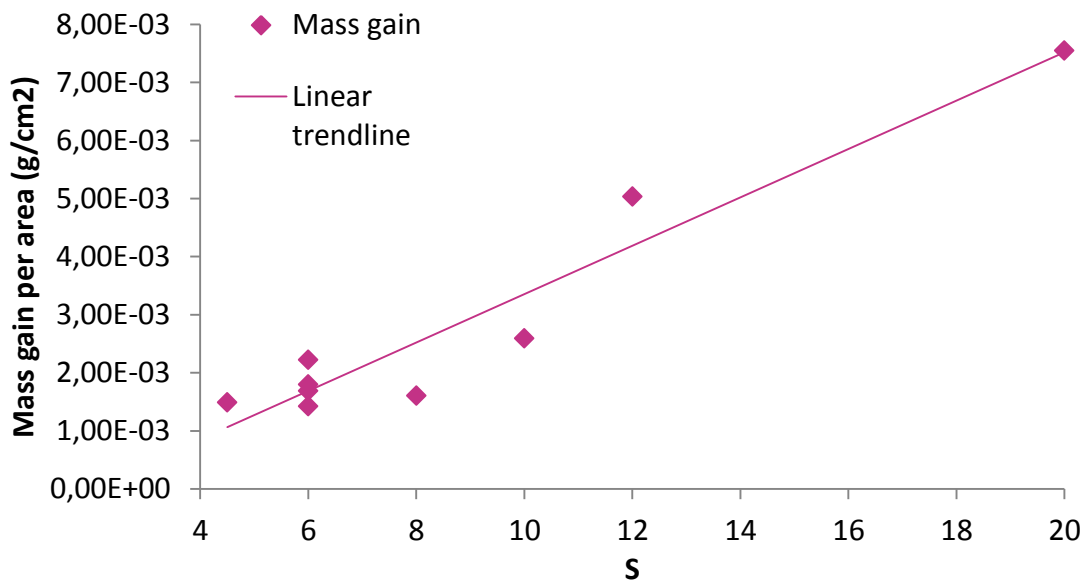
Figure 33: Relation between supersaturation and mass gain (90 minutes, T_{tube}=90°C, T_{bulk}=30°C)

The relationship between the mass gain and supersaturation indicates a linear relationship. When temperature is constant, the solubility product is also constant. An increase in dissolved species will give more precipitate. Higher supersaturations correspond to more available reactants in the solution and thus, more scale is formed.

A somewhat similar study was performed by Hasson et al. (1968). Here, the deposition rate was calculated as a function of the difference in calcium carbonate driving force. This driving force is expressed in ppm, without specifying the basis. Also, this driving force was calculated from a kinetic model developed for a pre-scaled surface. The deposition rate is therefore not directly comparable to the results in this study, but the trend of the rate can still be compared. A linear acceleration in growth rate of calcium carbonate was found as the excess of calcium ions at the scale interface increased (local supersaturation at the surface). Experimental conditions otherwise were bulk temperatures in the range 35-43°C and surface temperature 80-85°C.

It should be noted that the range of supersaturations in the present study is quite large. As seen in Figure 8, the growth mechanism changes with supersaturation and this impacts the growth rate. Hence, the linear relationship which Figure 33 indicates, is not expected to be valid for all ranges of supersaturations.

45

4.3 Temperature effect

Scale growth is impacted by temperature in many ways; via the kinetic parameter, by the solubility which decreases as temperature increases and through the degree of supersaturation, which also changes with temperature. Both the bulk liquid temperature and the surface temperature can influence the scale growth rate. Therefore, before determining such rates, the effect of each temperature should be revealed.

Again, the basis temperature used to calculate the initial supersaturation in this system is the bulk temperature. As the bulk temperature is increased, the initial composition of the mixed reactant solution varied to yield a constant initial supersaturation of S=6. When the surface temperature is changed, no corrections are done as the bulk temperature is still constant.

4.3.1 Impact of bulk temperature

The heated surface will have a boundary layer with decreasing temperature between the surface and the bulk fluid, as seen in Figure 15. The temperature of the boundary layer and the bulk fluid are defined as equal as the interface. When the temperature of the bulk fluid rises, the temperature difference is reduced. Thus, a different boundary layer with a different gradient is created between the surface and the bulk fluid. This could impact both the morphology and growth rate of the scale layer.

As seen in Figure 34, the mass gain increases slightly (and only for two of the experiments) when raising the bulk temperature from 30°C to 50°C. The increase between bulk temperature 50°C and 70°C is marginally.
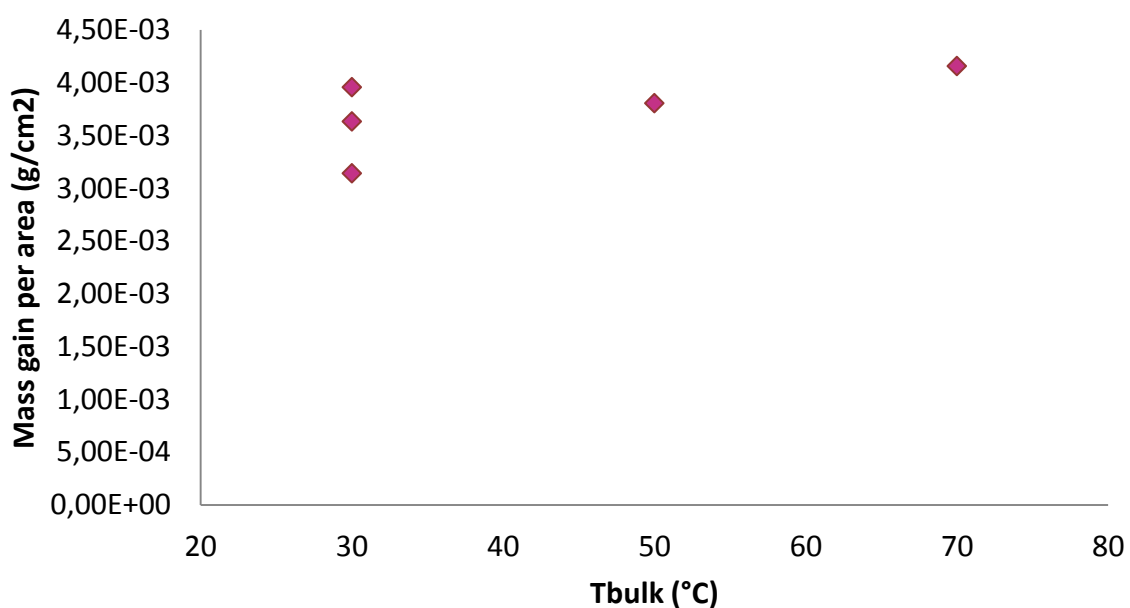

Figure 34: Mass gain per area as function of bulk temperature (S=6, T_{tube}=90°C, 180 minutes)

The small degree of impact from the bulk temperature can be made probable by kinetic considerations. The increased bulk temperature will speed up the kinetics governing mass transport (the diffusion coefficient) but have little direct effect on the kinetic parameter in the scale growth expression. Hence, if the growth is controlled by surface integration, an insignificant change in mass gain should be expected. The SEM-images from the experiment are given in Figure 35
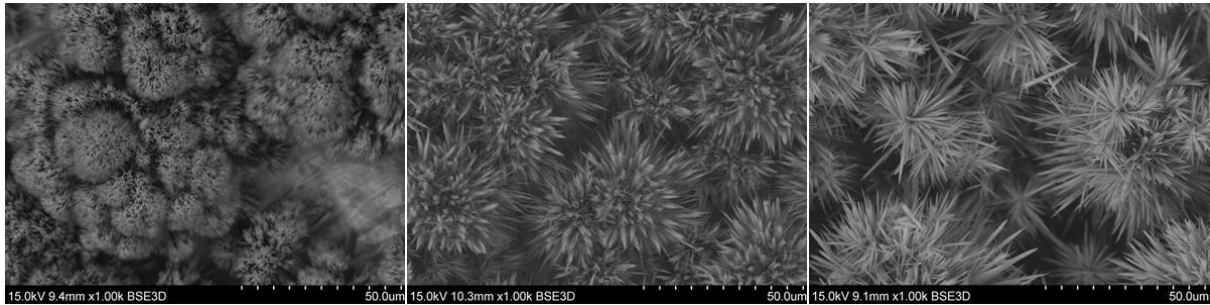

Figure 35: Bulk temperature 30°C (left), 50°C (middle) and 70°C (left) temperature (S=6, T_{tube}=90°C, 180 minutes). The image scale bar is 50 μm.

The SEM-photographs of the three experiments reveal that aragonite is formed in all experiments, but with a significant change in morphology as the conditions are altered. At T_{bulk}=30°C, agglomerates consisting of minor bouquets of aragonite-needles are seen. The length of the aragonite needles is less than 5μm and it is not possible to differentiate one needle from the other. By rising the bulk temperature to 50°C, the needle size increase radically. Now, each needle is separable, thicker and about 15μm long. The needles are attached to a spherical structure about 20 μm in diameter. As the bulk temperature is increased to 70°C, even more defined needles are found. The needles appear to grow from the same point in the structure in a type-1 spherulitic manner. The length of the needles is between 20-35 μm.

The change in morphology seen in Figure 35 indicates that the transport through the interface is impacted by the bulk temperature. Finer and more defined needles suggest that the incorporation of molecules into the crystal lattice is easier as the temperature difference is decreased

Morphology will also impact the stability of the scale layer as a whole. In Figure 35, the left image show some broken aragonite needles. These structures are clearly more porous than the structures formed at greater temperature differences relative to the surface temperature. The heat transfer through this porous structure will most probably be different from the heat transfer in a denser scale layer.

Also, these results indicate an important application for industrial purposes: porous and fragile scale is easier to destroy than a denser scale layer. This can make the scale layers

easier to remove, but also increase the amount of solids in the stream passing by the heat exchanger.

4.3.2 Effect of changing tube surface temperature

Tube surface temperature impacts the growth rate of calcium carbonate in two ways: The solubility product will decrease as the temperature increases and the growth rate constant will increase due to the Arrhenius dependence on temperature, as seen in Section 2.5.

Figure 36 show that the mass gain has an asymptotic behavior as tube surface temperature is increased. As expected, the deposition rate is close to 0 when no heat gradient between the tube and the bulk solution is applied (30°C). An increase in surface temperature from 50°C to 90°C resulted in 35% more mass deposited per area after 270 minutes. The mass increase is greatest for the temperature raise between 50°C to 70°C (28% difference); between 70°C and 90°C the difference is only about 7%.
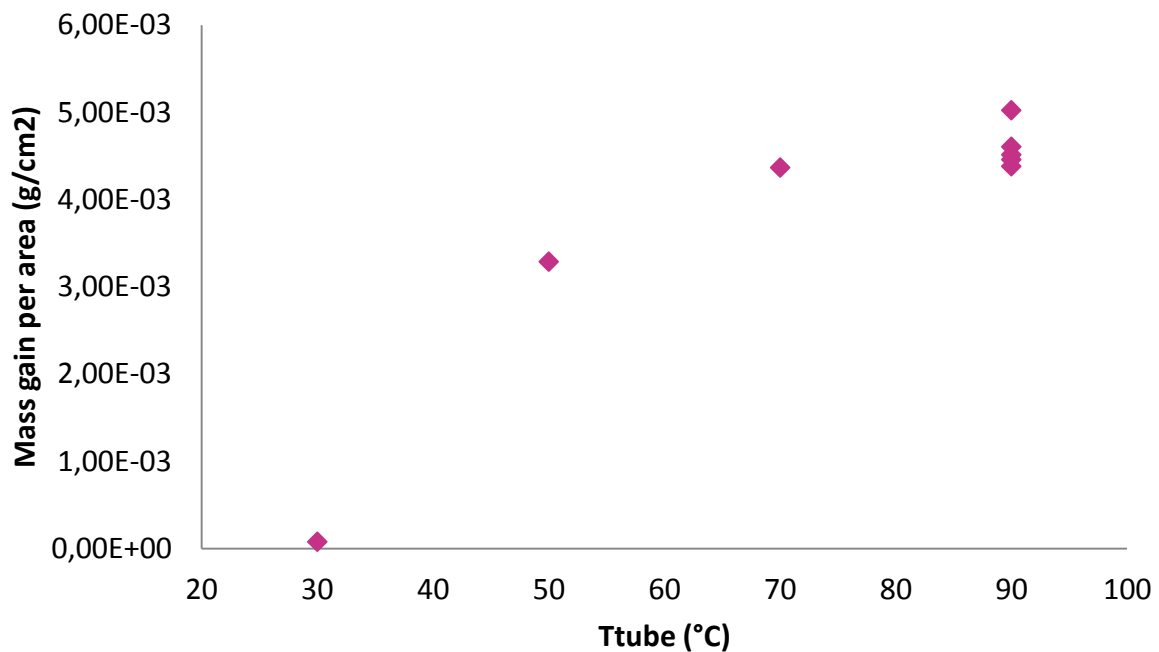
Figure 36: Mass gain per area as function of T_{tube} (S=6, T_{bulk}=30°C, 270 minutes)

Hasson et al. (1968) found a 20% increase in scale rate as temperature was raised from 64°C to 84°C when the bulk temperature was constant at 45°C. These experiments were performed at lower pH compared to the present study and at undefined supersaturation. Hence, they should only be used to support the discovery presented in the paragraph above; for constant bulk temperature, the scaling rate increases as the surface temperature is increased.

The SEM-pictures from the experiments in this study reveal another interesting discovery, as shown in Figure 37. At T_{tube}=50°C, a mix of calcite and aragonite is seen at the surface. For T_{tube}=70°C and 90°C, almost only aragonite is formed.
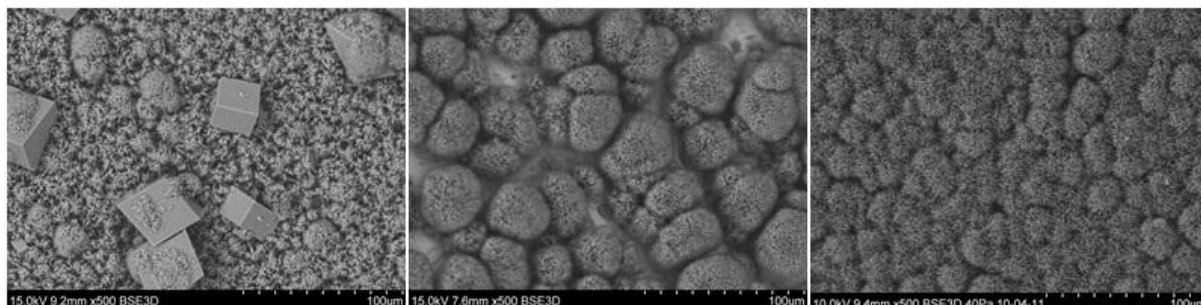
Figure 37: Scale deposited at surface temperatures of 50°C(left), 70°C (middle) and 90°C (right)(S=6, T_{bulk}=30°C, 270 minutes). The image scale bar is 100 μm.

Quantitative data for the different polymorphs were obtained by performing a Rietveld analysis in TOPAS on the XRD-spectra from these experiments. The result from the quantification analysis is listed in Table 5. Spectra are given in Appendix G.

Table 5: Polymorphic distribution at varying surface temperature

Polymorph (%)	50°C	70°C	90°C
Calcite	42.8	2.5	0.4
Vaterite	1.3	0.1	0.2
Aragonite	55.9	97.4	99.4

According to Kitano ((1962) via (Cowan and Weintritt, 1976)), precipitation from a bicarbonate solution should yield a mix of all polymorphs at 50°C, with vaterite as the dominating polymorph. Ogino et al. (1987) found that by transformation from amorphous calcium carbonate, a polymorphic mixture with aragonite domination and vaterite as the second-most formed polymorph, could be expected at 50°C. Above 70°C, both references expect an aragonite yield close to 100%, which is in accordance with the results obtained in this work. The low occurrence of vaterite is further discussed in Section 4.4.

4.4 Polymorphic stability

Vaterite is predicted to be found at 50°C but can (with the exception of some spherulites seen at S=20) only be spotted in the introductory layer in short-run experiments. As stated, vaterite is the least stable polymorph of calcium carbonate. Ogino et al (1987) showed that precipitate of amorphous calcium carbonate will transform into the metastable vaterite, further to aragonite and finally to the thermodynamical stable calcite.

In this work, dissolving vaterite has been observed at the surface in some experiments, see Figure 38. If vaterite at these conditions (T_{tube}=50°C, experiment length 270 minutes) are transforming into a more stable polymorph, this can explain why the polymorphic ratio of vaterite compared to the other polymorphs is negligible.
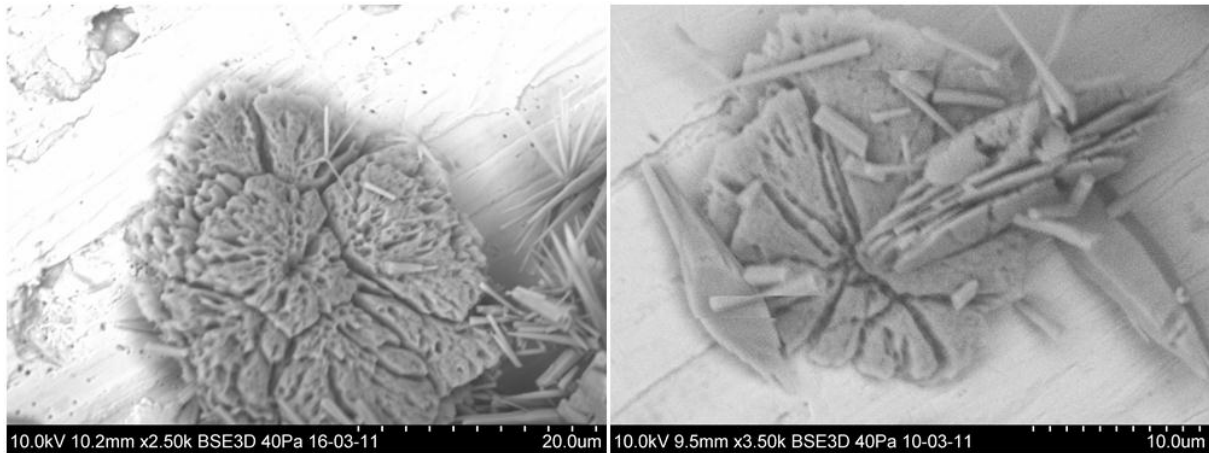
Figure 38: Dissolving vaterite at surface, S=8 (left) and S=6 (right) (Ttube=90, Tbulk=30, 180 minutes). The image scale bar is 10 µm.

Transformation of vaterite at similar conditions has been reported in literature: Spanos and Koutsoukos (1998) found that for the temperature range of 25-45°C, the conversion of vaterite into calcite was rapid and independent of pH and supersaturation. Hence, the thermodynamically stable polymorph was the one polymorph found in longer experiments. Also Andritsos et al. (1997) claims evidence of vaterite converting into aragonite and subsequently into calcite under isothermal scaling conditions.

In one experiment, the whole scale layer loosened from the heated tube, allowing inspection of the interface of scale layer to the surface. The resulting SEM pictures are shown in Figure 39.
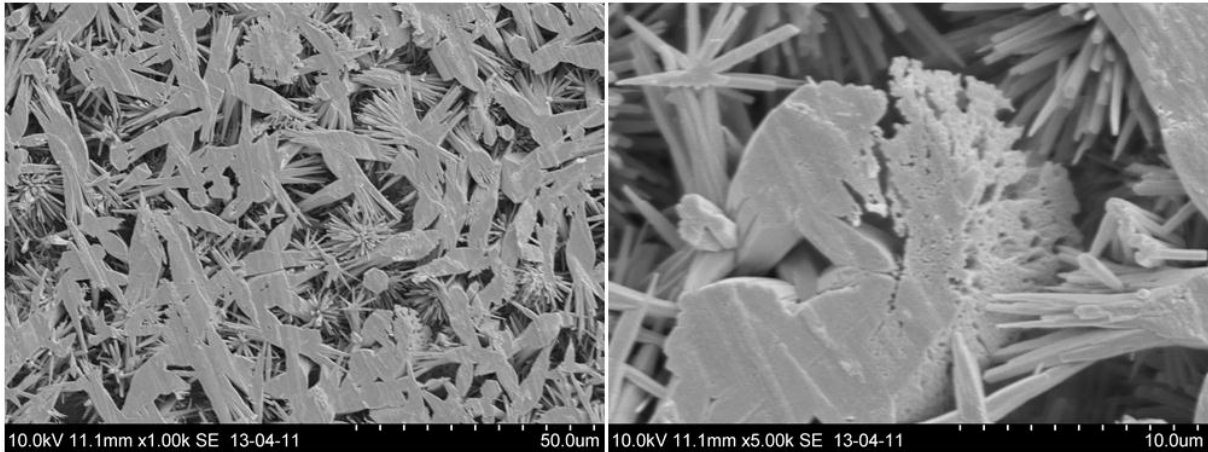
Figure 39: Scale layer seen from the surface (left) where vaterite in dissolution can be seen (right) (S=6, Ttube=90, Tbulk=30, 270 minutes). The image scale bar is 50 μm.

It is here evident how the scale layer is attached to the surface in only some points. Also here, dissolving vaterite is seen. It is noteworthy that the part of the crystallite in contact with the surface has dissolved less than the part growing into the aragonite dominated area (Figure 39, left). The amount of vaterite formed in the introductory phase can therefore impact the stability of the scale layer as a whole, as the surface adhesion will decrease as vaterite dissolves.

These discoveries highlight once more the importance of studying both kinetics and thermodynamics together. It is not known if aragonite, which also is a metastable polymorph, will transform at the conditions studied in this work.

4.5 Bulk nucleation

During the experiments, it was observed that the solution samples taken from the reactor at S=20, was turbid, whereas the samples at S=6, were clear (Figure 40). As discussed in Section 4.2, more scale was formed at S=20 then at S=6. Higher supersaturation means higher potential for precipitation when the solubility product is constant. However, this precipitation potential does not differentiate between precipitation in bulk and precipitation as scale formation. The observed suspended crystals can either origin from the scale formed at the tube or it can be particles nucleated in the bulk fluid in the reactor.

Figure 40: Opalescent bulk solution due to bulk precipitation at S=20 (left), clear bulk solution at S=6 (right)

During the experiments, equal volumes of bulk solution from experiments at S=20 and S=6 were filtrated. A visible layer of white crystals covered the filter from S=20, whereas no crystals were observed by eye for S=6. SEM-pictures from these filters are shown in Figure 41. For S=20, a small selection of the loose crystal powder were deposited onto carbon tape, whereas the filter itself was investigated for S=6.
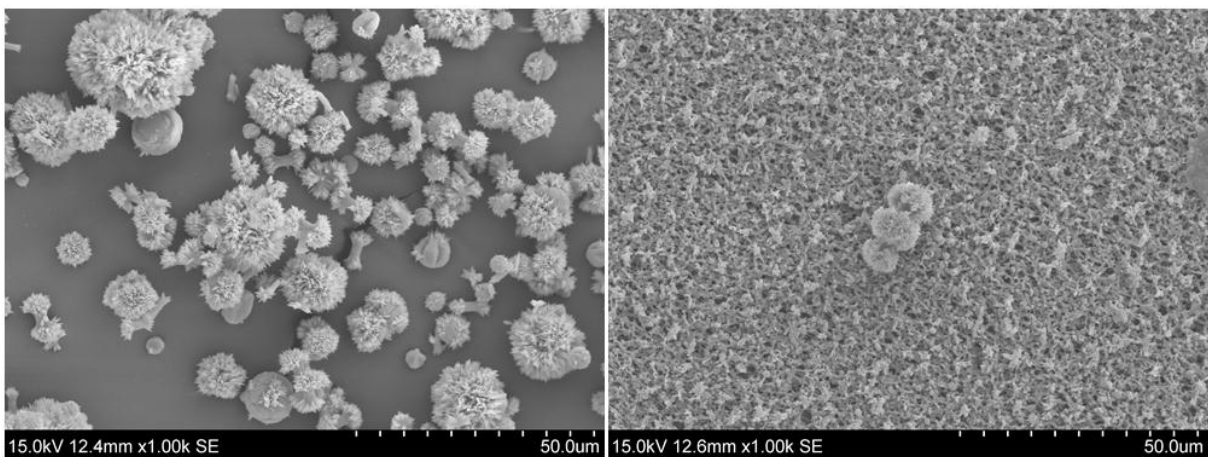
Figure 41: Bulk precipitation at S=20 (left) and S=6 (right) (Ttube=90C, Tbulk=30C, after 60 min (S=20) and 300 min (S=6)). Scale bar is 50 µm.

At S=20, aragonite is the dominating polymorph, but some vaterite plates and spherulites can also be observed. Aragonite is only seen in spherulitic form. Several different stages of typeII-spherulitic growth can be seen. As shown previously in Figure 32, spherulites of aragonite were also seen in between the dendritic structure growing form the surface. The

52

difference in morphology between the particles found in bulk and at the heated surface can indicate that bulk nucleation is occurring, rather than scale particles loosening from the tube. At the surface, the crystallites have a layered dendritic structure, whereas the bulk precipitate consists solely of separate crystallites.

Bulk nucleation can be a result of homogeneous nucleation as the precipitation potential is high at high supersaturations. As shown in Section 2.10, dead zones exist in a stirred reactor with baffles fastened on the wall. In these zones, the bulk fluid is more stagnant and does not only act as a serving medium towards the heated surface. It is possible to look at the bulk fluid here as an individual surface, upon where the reactants nucleate more easily at higher supersaturations.

In Table 11, the presented effective supersaturation was calculated. The effective steady state supersaturation in close vicinity (90°C) to the heated surface was reduced from the initial S=20 to S=8.5, a reduction of almost 130%. For S=6, the corresponding difference between initial and effective steady state supersaturation was 35% as S reduced to 5.2. This points towards a threshold in supersaturation; above this, bulk nucleation will consume most of the excessive supersaturation introduced to the system.

A study referred to by Cowan and Weintritt (1976) showed that for a natural brine at a temperature of 90°C, only one third of the calcium precipitated would be in form of scale on the surface. As the temperature was decreased, less mass was precipitated but a greater fraction was scale. At 50°C, about 90% of the precipitate was scale. The early results from the experiments in the present study, point towards a similar relationship between total amounts of precipitate (as indicated by the drop in calcium concentration), scale and decreasing supersaturation.

4.6 Scale growth rate of aragonite

Table 5 revealed how experiments conducted with tube temperature at 90°C yielded >99% aragonite, enough to consider the scale as pure aragonite. Hence, scale growth rate for aragonite only can be determined.

A range of experiments at S=20 and S=6 were completed for T_{tube}=90°C, T_{bulk}=30°C and varying experiment length. This surface temperature was chosen to be sure aragonite was yielded. As seen in Section 4.2.2, more scale would be formed for S=20 compared to S=6 for the same experimental length. Hence, shorter experiments were conducted for S=20 than S=6.

As Figure 42 illustrates, both S=6 and S=20 show an initial linear relationship between mass gain and time. For S=20, the curve flattens out after the deposited mass reaches 0.012

g/cm^2. This early-asymptotic behavior can indicate that the heat transfer through the deposited layer decreases, thus slowing down the growth rate.
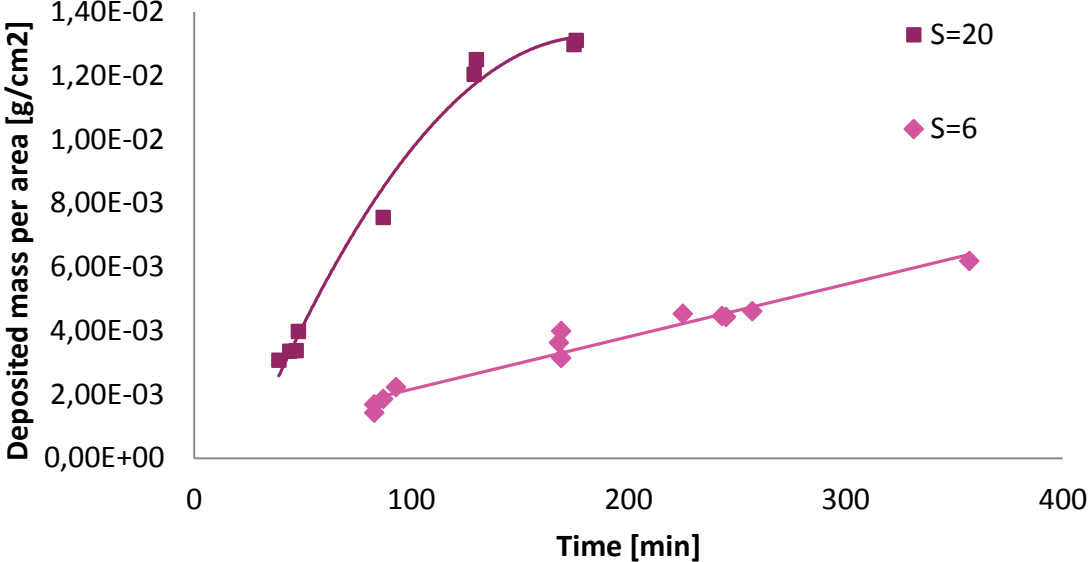

Figure 42: Mass gain as function of time (T$_{tube}$=90°C, T$_{bulk}$=30°C)

A plot of the deposition rate with time, support this hypothesis further; see Figure 43 below.
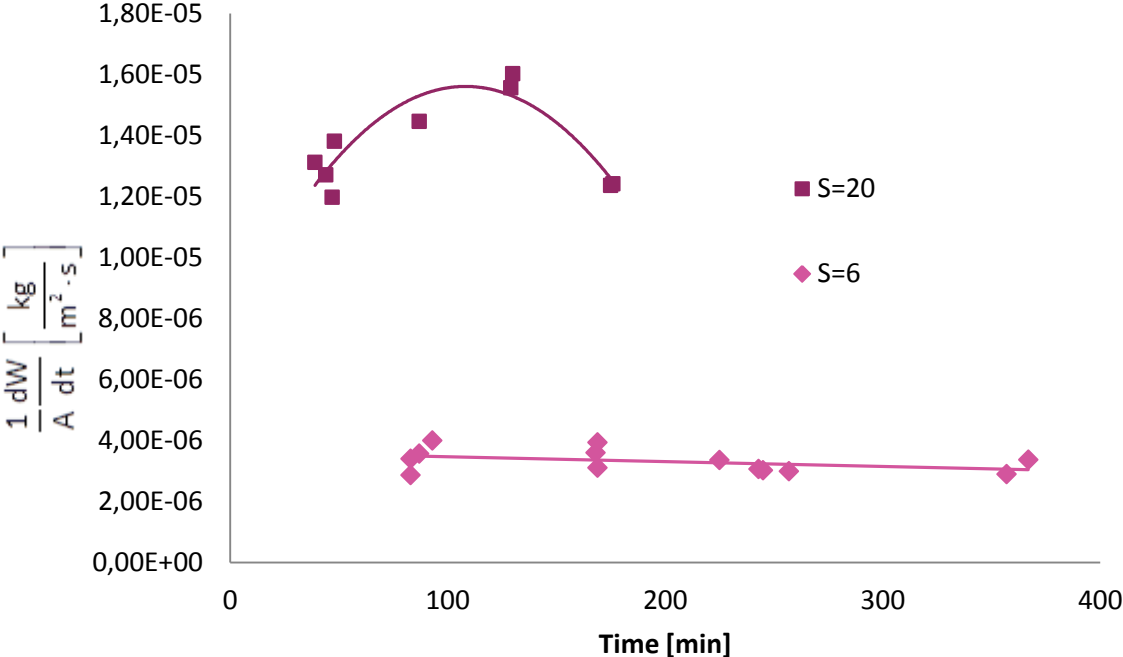
Figure 43: Scale growth rate (Ttube=90°C, Tbulk=30°C)

Converting the data from Figure 42, given in Figure 43, to growth rates reveals how the scale growth rate for S=6 is virtually constant over the experiment length. The growth rate for S=20 increases steadily until it suddenly drops. Reduced heat transfer can, as mentioned, explain the drop.

Two possible reasons for the initial increase in growth rate at S=20 are local variations in supersaturation and self-accelerating growth due to increased branching and greater scaling area. As the temperature at the scale tip decreases, the supersaturation actually increases slightly. This is a result of the complex equilibria for the calcium carbonate as temperature changes and is further discussed in Appendix F.

Figure 44 show how the difference in morphology between S=6 and S=20 after 180 and 135 minutes, respectively.
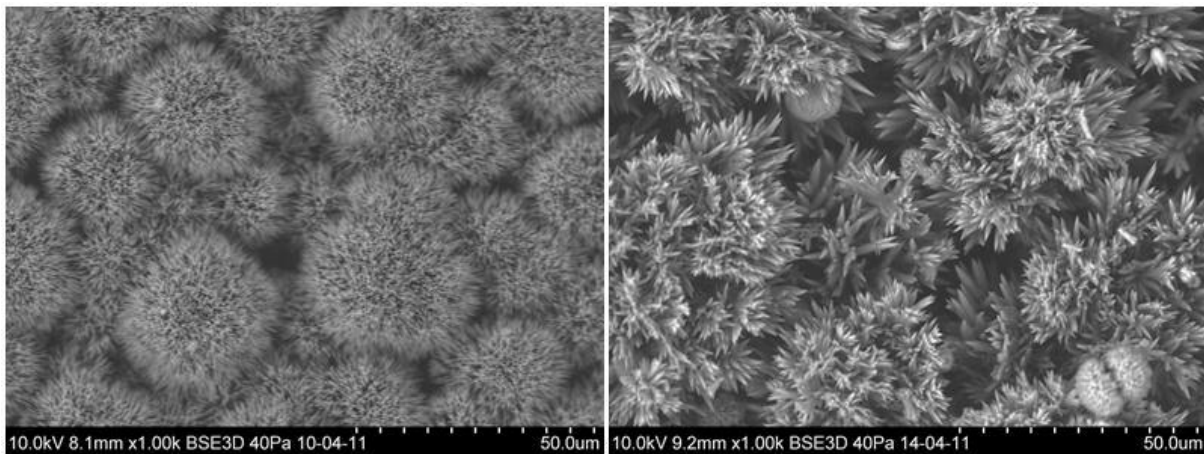
Figure 44: S=6 after 180 min (left) and S=20 after 135 minutes (right) (T_{tube}=90°C, T_{bulk}=30°C). The image scale bar is 50 μm.

The aragonite needles at S=6 are small (<5μm), very thin and are closely packed together in spherical agglomerates. At S=20 the structure is more open. Each needle is defined, thicker and has a length about 15 μm. Actual scaling area will be is the area of all the crystal faces exposed to reactants and available for integrating these into the lattice. At high supersaturations, the diffusion of reactants towards the surface is large as the driving force is large (Figure 15). As more reactants are incorporated into the crystal structure, even more supersaturation is consumed due to the increased area resulting from increased branching. This process accelerates itself and causes the scale growth rate to increase. Since the exposed area at S=6 is smaller, this self-acceleration do not occur at this supersaturation.

In literature, scale growth rates for solely aragonite are not found for aragonite. Instead, linear growth rates for aragonite in bulk solutions in batch experiments will be compared to the growth rates from this work in the following section.

4.7 Linear growth rate of aragonite

Aragonite scale consists of thousands of agglomerates of monocrystalline aragonite needles. After the surface is covered by the initiating scale layer, further growth in lateral direction will be restricted. Thus, scale growth is favored in z-direction; perpendicular to the surface. This is also the direction where the supply of reactants is greatest.

Crystals growing in bulk often have a preferred direction of growth. As discussed in Section 2.7, for aragonite, two of the faces grow faster than the other, resulting in a needle-shaped crystal. Linear growth rates for aragonite in bulk are averaged over all the faces of the aragonite crystal.

Bulk growth and scale growth are two different mechanisms. However, comparing the bulk growth rate of aragonite to the scale growth rate of aragonite agglomerates, can give information on what impact the heated surface actually has on the growth rate and the growth mechanism.

4.7.1 Conversion from scale growth rate to linear rate

In order to convert the deposition rate based on mass to a linear rate, a density value is required. Using the crystalline density of aragonite would require the scale layer to be completely dense. As discussed, scale is usually a porous structure with void spaces in between the crystal depositions. Hence, the density of the scale layer is lower than the crystalline density and should be estimated. This can be done using the deposited mass and an estimate of the scale volume. Following assumptions were made:

- o The surface area of the tube is set as scaling area. This corresponds to averaging all crystal faces in a spherical cross section around the tube, as a rough approximation
- o Radial increase in area is neglected. Hence, the scaling area is equal to the surface area of the tube in all radial positions
- o The scale layer has the same height over the whole area
- o Mass is uniformly distributed over the area
- o Polymorphs other than aragonite are neglected (valid approximation as these accounts for less than 1% of the polymorphs at 90°C)
- o Scale density is independent of supersaturation, in other words: the porosity is the same for S=6 and S=20. This is also a rough approximation and it is possible that this gives a too low density for S=6.

Using these assumptions, only the thickness (height) of the scale area is required to be able to estimate the volume and thus, the density of the scale layer.

Figure 45 show how a precise cut into the tube surface allowed the height of the agglomerate structures to be calculated by the SEM-software. The density was estimated from the average height of the branched structures in each experiment.
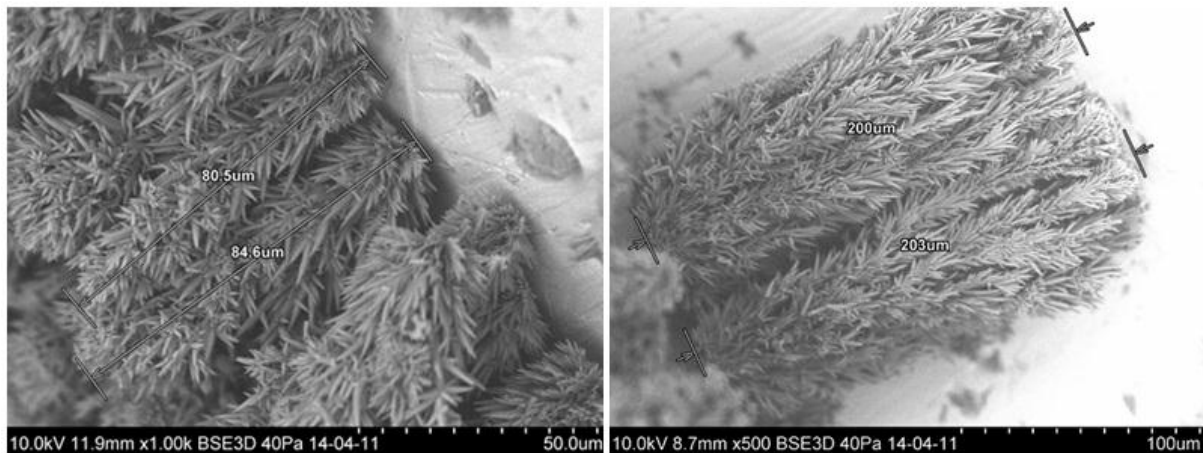
Figure 45: Scale thickness, S=20, experiment length 39 min (left) and 130 min (right). The image scale bar is 100 µm.

Then, as seen in Table 6 below, the two densities were also averaged in order to yield an overall average density.

Table 6: Density of aragonite scales

S=20	39 min	130 min	Average
Calculated density (g/cm^3)	1.9	2.1	2.0
Theoretical density	2.9		

The estimated density suggests that about 30% of the scale layer is void space. Looking at the deposited layers in Figure 45, this seems reasonable.

As expected, the plot in Figure 46 differs from the corresponding figure in Section 4.5 only by a constant. The linear growth unit is now in m/s. For S=6, these experiments give a linear growth rate about 5 nm/s. As discussed, the growth rate for S=20 is changing over time, but an average rate is found to be around 22 nm/s .
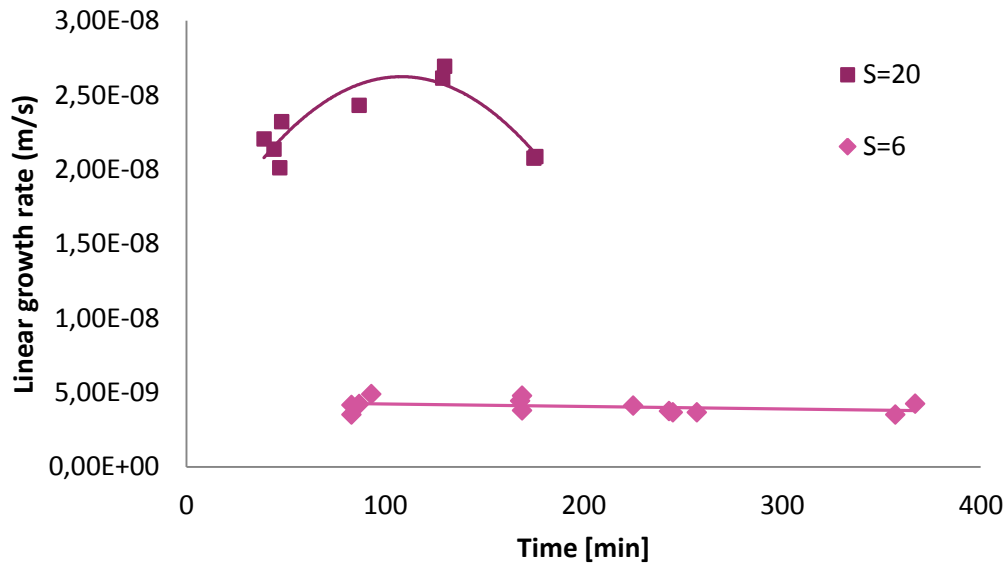
Figure 46: Linear growth rate (T_{tube}=90°C, T_{bulk}=30°C)

4.7.2 Comparison with literature

Mersmann and Kind (via (Mullin, 2001)) reported on growth rates for calcium carbonate in the range of 10^{-8}-10^{-9}m/s. It is not specified at what temperature and for which polymorph these results are valid. Three studies where linear growth rates of aragonite were determined from batch experiments were found:

One of the first studies on aragonite growth rates was performed by Gutjahr et al. (1996). Here, growth rate parameters are given for two different stoichiometric ratios of calcium chloride and sodium bicarbonate and for different temperatures. In order to convert the growth rate from the given units to nm/s, the theoretical density of aragonite is used. The two growth rate constants and growth orders for aragonite at 70°C are averaged to give the expression $G=122.0(S^2-1)^{1,53}$ nm/s , where S^2 arises from a different definition of supersaturation.

Flaten et al. (2010) performed aragonite growth experiments by adding seed aragonite crystals to a solution of calcium chloride saturated by carbonate from CO_2-bubbeling. The temperature range studied was 40°C to 70°C and the supersaturation was below 3 with respect to vaterite. For aragonite, the generalized linear growth rate expression was given as $G=0.9(S-1)^{3,52}$ nm/s .

Also Olderoy et al. (2011) performed seeded growth experiments with CO_2-bubbeling at 40°C. Supersaturation with respect to calcite at 40°C was 5.3. For aragonite, the growth

constant, k_g, was found to be 0.021 nm/s. The growth order is not given by the authors, so a growth order of 2.0 is assumed. This is the general growth order for polynuclear growth, indicated as regime C in Figure 8 in Subsection 2.5.3 and chosen as no dendritic structures are seen in this work.

When inserting the steady state supersaturation of aragonite at 90°C, the expressions from literature should give growth rates for aragonite comparable to the rates determined experimentally in this work, see Table 7.

Table 7: Comparison between bulk growth rates (obtained in this work) and linear scale growth rates (calculated from literature) for aragonite, all rates given as m/s

Growth rates (m/s)		Gutjahr et al. (1996)	Flaten et al. (2010)	Olderoy et al. (2011)	This work
$S_{calcite}$ initial at 30°C	$S_{aragonite}$ steady state at 90°C				
6	4.4	1.0E-05	6.5E-08	2.4E-10	5.0E-09
20	7.2	5.1E-05	5.7E-07	8.2E-09	2.2E-08

The results from this work is obtained at 90°C, whereas the literature expressions are valid for 70°C, 40-70°C and 40°C, respectively. Hence, slightly lower growth rates would be expected for the calculated rates, as Figure 36 revealed that the mass gain increased with increasing temperature. However, as Table 7 show, this is not the case.

Growth rate expressions from Gutjahr et al. and Flaten et.al both give higher growth rates than the one obtained in this work. This can be explained by the three different growth rate regimes introduced in Figure 8. Which regime the growth rate data is obtained from, will determine the growth order. Hence, data obtained in regime B where two dimensional growth take place, will give a totally different growth order and following, growth rate, than data obtained in regimes of spiral or rough growth. The data from Olderoy et al. are obtained at 40°C only, which can be one of the explanations of the slow growth.

Growth rate studies should be performed over a large range of supersaturations to capture the different growth regimes. To expect that one general growth rate expression can give accurate values for all three regimes of crystal growth, is most probably a rash expectation. The effect of heat transfer on the crystal growth rate relative to bulk growth rate can therefore not be determined by this work. A more thoroughly study of growth rates from bulk experiments should be conducted for a greater selection of supersaturations. If a growth rate expression for the same growth mechanism as the mechanism of scale growth (dendritic rough growth) can be obtained, the experimental and calculated growth rate can be compared.

5 Conclusions

The experimental setup developed let the scaling parameters pH, calcium concentration and bulk temperature arrive at a steady state where the parameters are constant, resulting in a constant supersaturation. A continuously stirred tank is used which gives the same supersaturation for all scaling points. This way the setup simulates industrial heat exchange well and allows tuning of important scale parameters.

An onset of scale formation was found around S=4.5 with respect to calcite. In accordance with general fouling theory, lateral growth took place during the initiation period. Other polymorphs than aragonite was found in the lateral scale layer compared to the outward directed growth. This outward directed growth occurred after the surface was completely covered by scale.

Increasing the supersaturation increased the mass precipitated as scale. Morphology of the crystals was also impacted by the increased supersaturation; larger and less uniform structures were found at higher degree of supersaturations. It is likely that the relationship between supersaturation and mass gain changes with supersaturation, as the growth model changes towards diffusion controlled growth at high supersaturations.

As the tube surface temperature was increased from 50°C to 90°C, the deposited mass increased by 35%. Also the polymorphism changed. At tube temperature 50°C, 43% calcite and 56% aragonite was formed. As temperature was increased to 70°C, 97% of the scale content was aragonite and at 90°C, more than 99% aragonite was formed. Less vaterite than predicted by literature was found. Vaterite in the process of dissolving was seen after 180 minutes. Thus, the type of polymorphs formed in the introductory scale layer can therefore be important for the long-time stability of the scale layer as a whole.

Increasing the bulk temperature when the tube surface temperature was fixed had little impact on the amount of deposited mass. However, the morphology was clearly impacted. The scale units increased in size and the scale structure as a whole became more porous and fragile, as the temperature difference relative to the tube was decreased.

Extensive bulk nucleation occurred at high supersaturations, whereas almost no bulk nucleation was seen at lower supersaturations. The effective steady state supersaturation in close vicinity to the heated surface was reduced from the initial by value almost 130% for the high supersaturation, compared to 35% for the lower. This points towards a threshold in supersaturation; above this limit, bulk nucleation will consume most of the excessive supersaturation introduced to the system.

Since only (>99%) aragonite was found at 90°C, the experimental setup could be used to determine growth rates of aragonite. Such growth rates are rare for batch experiments and

not found for scaling experiments. The scale growth rate was found to have a parabolic shape for high supersaturations and to be constant for lower supersaturations, which can be a result of different growth regimes. The scale growth rate for high supersaturation (S=20) was between 1.2E-5 and 1.6E-5 kg/m^{2}s. For the lower supersaturation (S=6), a constant scale growth rate of 3.5E-6 kg/m was found.

In order to compare scale growth rates to growth rates from batch experiments, the scale growth rate must be converted to a linear rate. Growth rate expressions for growth limited by surface reaction yield a different growth order (and rate) than a diffusion controlled growth rate expression. Hence, the growth regime in which the growth rates are obtained should be equal for the comparison to be valid.

Suggestions for future work

In this work, the scaling parameters temperature and supersaturation have been varied. One of the important engineering parameters for continuous systems with steady state is the residence time. The effect of changing residence time should be investigated in order to increase the understanding of scaling at industrial conditions.

This work has been performed using stoichiometric amounts of reactants. As literature indicates that stoichiometry can influence the polymorph formed, this should be tested in this setup.

As already mentioned, a thoroughly study of growth rates at different supersaturation can give the required information to construct growth rate expressions for scaling at heat exchangers. Different surface temperatures should also be tested.

When processing natural gas, antifreeze agents such as mono ethylene glycol (MEG) are present together with the water. It has been demonstrated that addition of MEG changes the polymorphism for particles in bulk experiments. This knowledge should be transferred to the continuous scaling system developed to see if the same results are predicted by this setup.

If possible, regimes where only calcite and vaterite exist should be identified and growth rate expressions obtained for these polymorphs. When the growth rate expressions for each polymorph are known, this information can be coupled with the current process conditions. This knowledge can also be used to design additives which switch the polymorphism towards the slowest growing. Inhibitors currently in use should be tested towards the polymorphs expected for those conditions to quantify what effect they really have on scaling.

List of symbols

Symbol	Unit	Name
A	1) - 2) varies	1) Proportional constant 2) Pre-exponential kinetic parameter
A_T	-	Total alkalinity
a	-	Activity
$a_{\pm}$	-	Mean ionic activity
a^*	-	Activity at equilibrium
B	Varies	Pre-exponential kinetic parameter
c	$\frac{mol}{L}, \frac{mmol}{kg_{solvent}}$	Concentration
c^*	$\frac{mol}{L}$	Equilibrium concentration
c_p	$\frac{J}{K \cdot mol}$	Heat capacity
F	$\frac{g}{m^3}$	Flow
G	1) $\frac{J}{mol}$ 2) $\frac{m}{s}$	1) Gibbs free energy 2) Growth rate
g	-	Growth order
γ	1) - 2) N/m 3) m^2	1) Activity coefficient 2) Interfacial tension between liquid and crystal 3) Heat transfer area
$\gamma_{\pm}$	-	Mean activity coefficient
h	$\frac{W}{m^2 \cdot K}$	Convective heat-transfer coefficient
I		Ionic strength
J	$\frac{mol}{s \cdot L}$	Nucleation rate
K_g	-	Overall growth rate constant

K_{sp}	-	Equilibrium solubility product
k	1) $\frac{J}{K}$ 2) $\frac{W}{m^2 \cdot K}$	1) Boltzman constant 2) Thermal conductivity
k_g	-	Growth order constant
κ	m	Thickness of a 2-D nucleus
L	m	1) Characteristic length of a particle 2) Length of a cylinder
M	$\frac{g}{mol}$	Molar mass
m	g	Mass
n	mol	Moles
q	$\frac{J}{mol}$	Heat transfer rate
Q	J	Heat transfer rate
R	$\frac{J}{mol \cdot K}$	Universal gas constant
r	m	Radius
S	-	Supersaturation ratio
t	S, min	Time
T	K	Temperature
τ	s	Residence time
θ	°	Contact angle
U	$\frac{W}{m^2 \cdot K}$	Overall heat transfer coefficient
μ	$\frac{J}{mol}$	Chemical potential
V	m^3(SI), mL(here)	Volume
v_0	$\frac{m^3}{s}$	Volumetric flow
ν	-	Number of moles in one mole electrolyte solution
z_i	-	Charge number of specie i

References

ANDREASSEN, J.-P. 2010. Short course on precipitation and crystallization from solution. Trondheim: NTNU.

ANDRITSOS, N. & KARABELAS, A. J. 2003. Calcium carbonate scaling in a plate heat exchanger in the presence of particles. *International Journal of Heat and Mass Transfer,* 46**,** 4613-4627.

ANDRITSOS, N., KARABELAS, A. J. & KOUTSOUKOS, P. G. 1997. Morphology sand structure of CaCO3 scale layers formed under isothermal flow conditions. *Langmuir,* 13**,** 2873-2879.

BANSAL, B., CHEN, X. D. & MÜLLER-STEINHAGEN, H. 2008. Analysis of [`]classical' deposition rate law for crystallisation fouling. *Chemical Engineering and Processing: Process Intensification,* 47**,** 1201-1210.

BAZIN, B., KOHLER, N. & ZAITOUN, A. 2005. Some Insights Into Tube Blocking Test Method To Evaluate the Efficiency of Scale Inhibitors. *Society of Petroleum Engineers,* 96560.

BOTT, T. R. 1995. *Fouling of heat exchangers*, Elsevier.

BOTT, T. R. 1997. Aspects of crystallization fouling. *Experimental Thermal and Fluid Science,* 14**,** 356-360.

CALLISTER, W. D. 2007. *Materials Science and Engineering. An introduction*, John Wiley & Sons, Inc.

CAO, G. & WANG, Y. 2011. *Nanostructures and nanomaterials: synthesis, properties, and applications,* New Jersey, World Scientific.

CHEN, T., NEVILLE, A. & YUAN, M. 2005. Calcium carbonate scale formation--assessing the initial stages of precipitation and deposition. *Journal of Petroleum Science and Engineering,* 46**,** 185-194.

COWAN, J. C. & WEINTRITT, D. J. 1976. *Water-formed scale deposits,* Houston, Tex., Gulf Pub. Co., Book Division.

CRABTREE, M., ESLINGER, D., MILLER, M., FLETCHER, P., JOHNSON, A. & KING, G. 1999. Fighting scale - Removal and Prevention. *Oilfield Review,* 3.

ELLIOTT, S. R. 1998. *The physics and chemistry of solids,* Chichester, Wiley.

FAHIMINIA, F., WATKINSON, A. P. & EPSTEIN, N. 2007. Early events in the precipitation fouling of calcium sulphate dihydrate under sensible heating conditions (vol 85, pg 679, 2007). *Canadian Journal of Chemical Engineering,* 85**,** 948-948.

FLATEN, E.-M., SEIERSTEN, M. & ANDREASSEN, J.-P. 2009. Polymorphism and morphology of calcium carbonate precipitated in mixed solvents of ethylene glycol and water. *Journal of Crystal Growth,* 311**,** 3533-3538.

FLATEN, E.-M., SEIERSTEN, M., SIVANESAN, V. & ANDREASSEN, J.-P. 2010. Precipitation of calcium carbonate in mono ethylene glycol and water. Department of Chemical Engineering, NTNU

Institute for Energy Technology.

FOGLER, H. S. 2005. *Elements of chemical reaction engineering,* Upper Saddle River, N.J., Prentice-Hall PTR.

GRANASY, L., PUSZTAI, T., TEGZE, G., WARREN, J. A. & DOUGLAS, J. F. 2005. Growth and form of spherulites. *Physical Review E,* 72.

GUTJAHR, A., DABRINGHAUS, H. & LACMANN, R. 1996. Studies of the growth and dissolution kinetics of the CaCO3 polymorphs calcite and aragonite .1. Growth and dissolution rates in water. *Journal of Crystal Growth,* 158**,** 296-309.

HASSON, D., AVRIEL, M., RESNICK, W., ROZENMAN, T. & WINDREICH, S. 1968. Calcium carbonate scale deposition on heat transfer surfaces. *Desalination,* 5**,** 107-119.

HELBÆK, M. & KJELSTRUP, S. 2006. *Fysikalsk Kjemi,* Bergen, Fagbokforlaget.

INTERNATIONAL CENTRE FOR DIFFRACTION DATA 2011.

JAKOBSEN, H. A. 2008. *Chemical reactor modeling: multiphase reactive flows,* Berlin, Springer.

KARABELAS, A. J. 2002. Scale formation in tubular heat exchangers--research priorities. *International Journal of Thermal Sciences,* 41**,** 682-692.

KASHCHIEV, D. & VAN ROSMALEN, G. M. 2003. Review: Nucelation in solutions revisited. *Cryst. Res. Technol.,* 38**,** 555-574.

KEYSAR, S., SEMIAT, R., HASSON, D. & YAHALOM, J. 1994. Effect of Surface Roughness on the Morphology of Calcite Crystallizing on Mild Steel. *Journal of Colloid and Interface Science,* 162**,** 311-319.

KHAN, M. S., ZUBAIR, S. M., BUDAIR, M. O., SHEIKH, A. K. & QUDDUS, A. 1996. Fouling resistance model for prediction of $CaCO_3$ -scaling in AISI 316 tubes. *Heat and Mass Transfer,* 32**,** 73-79.

KITANO, Y. 1962. A STUDY OF THE POLYMORPHIC FORMATION OF CALCIUM CARBONATE IN THERMAL SPRINGS WITH AN EMPHASIS ON THE EFFECT OF TEMPERATURE. *Bulletin of the Chemical Society of Japan,* 35**,** 1980-1985.

MULLIN, J. W. 2001. *Crystallization,* Oxford Boston Butterworth-Heinemann.

MULTISCALE. 2010. Available: http://multiscale.no.

NANCOLLAS, G. H. The nucleation and growth of scale crystals. *In:* BRYERS, R. W., ed. Fouling of Heat Exchanger Surfaces, 1983. United Engineering Trustees Inc.

OGINO, T., SUZUKI, T. & SAWADA, K. 1987. The formation and transformation mechanism of calcium carbonate in water. *Geochimica et Cosmochimica Acta,* 51**,** 2757-2767.

OLDEROY, M. O., XIE, M. L., STRAND, B. L., DRAGET, K. I., SIKORSKI, P. & ANDREASSEN, J. P. 2011. Polymorph Switching in the Calcium Carbonate System by Well-Defined Alginate Oligomers. *Crystal Growth & Design,* 11**,** 520-529.

PARSIEGLA, K. I. & KATZ, J. L. 1999. Calcite growth inhibition by copper(II) I. Effect of supersaturation. *Journal of Crystal Growth,* 200**,** 213-226.

PLUMMER, L. N. & BUSENBERG, E. 1982. The solubilities of calcite, aragonite and vaterite in CO2-H2O solutions between 0 and 90°C, and an evaluation of the aqueous model for the system CaCO3-CO2-H2O. *Geochimica et Cosmochimica Acta,* 46**,** 1011-1040.

RANKIN, B. H. & ADAMSON, W. L. 1973. Scale formation as related to evaporator surface conditions. *Desalination,* 13**,** 63-87.

RIETVELD, H. M. 1969. A PROFILE REFINEMENT METHOD FOR NUCLEAR AND MAGNETIC STRUCTURES. *Journal of Applied Crystallography,* 2**,** 65-&.

SKOGESTAD, S. 2003. *Prosessteknikk: Masse- og energibalanser*, Tapir Akademisk Forlag.

SPANOS, N. & KOUTSOUKOS, P. G. 1998. The transformation of vaterite to calcite: effect of the conditions of the solutions in contact with the mineral phase. *Journal of Crystal Growth,* 191**,** 783-790.

SUNAGAWA, I. 2005. *Crystals: growth, morphology, and perfection,* Cambridge, Cambridge University Press.

TOLCHARD, J. 2010. *RE: Responsible engineer for the SEM and XRD labs.*

WOLFS, F. L. H. *Error analysis* [Online]. Available: http://teacher.pas.rochester.edu/PHY_LABS/AppendixB/AppendixB.html.

WU, Z., FRANCIS, L. & DAVIDSON, J. 2009. Scale formation on polypropylene and copper tubes in mildly supersaturated tap water. *Solar Energy,* 83**,** 636-645.

YANG, Q., LIU, Y., GU, A., DING, J. & SHEN, Z. 2002. Investigation of induction period and morphology of $CaCO_3$ fouling on heated surface. *Chemical Engineering Science,* 57**,** 921-931.

ZHANG, Y., SHAW, H., FARQUHAR, R. & DAWE, R. 2001. The kinetics of carbonate scaling--application for the prediction of downhole carbonate scaling. *Journal of Petroleum Science and Engineering,* 29**,** 85-95.

Appendix

A   Chemicals

In Table 8 below, the chemicals used in this work is listed.

Table 8: Applied chemicals

Chemical	Formula	State	Purity (%)	Supplier
Ammonia	NH_3	L	>25	VWR
Ammonium chloride	NH_4Cl	S	>99.5	Sigma
Calcium chloride dihydrate	$CaCl_2 \cdot 2H_2O$	S	99-103	Fluka
Ethylenediaminetetaacetic acid (EDTA)	$C_{10}H_{16}N_2 \cdot 2H_2O$	Aq	Titrisol(III)	Merck
Ethanol	C_2H_5OH	Aq	96	Sigma-Aldrich
Hydrochloric acid (used diluted)	HCl	L	37 (fuming)	Merck
Potassium chloride	KCl	S	>99.5	Merck
Sodium carbonate anhydrous	Na_2CO_3	S	≥99	Fluka

B   Pump capacity and deviation from stoichiometric conditions

In this work, two peristaltic pumps were used. This appendix will further describe the operation of the pumps and challenges related to these.

Pump capacity was not set directly, but as a value on a speed gear drive at pump B. From reactant volumes, solution densities and the duration of the experiment, the average pump capacity for this value was calculated. Also, the performance of pump B increased during the months the experiments were conducted. This was solved by adjusting the speed value after experiments where the calculations gave a different pump capacity than the desired, constant value. The last experiments were performed at speed value 8.5. Hence, the variation in peristaltic pump capacity in Table 1, Section 3.3 corresponds to the range of calculated pump capacities for the whole series of experiments (670±60 g/min)

Each peristaltic pump had two channels operated by the same gear wheel. Ideally, the two channels should deliver the same capacity. However, it was found that this was not the case. The average deviation was 0.78% surplus of one of the reactants. At the greatest, 2.55% deviation was registered. It was not consistent which reactant was delivered in surplus.

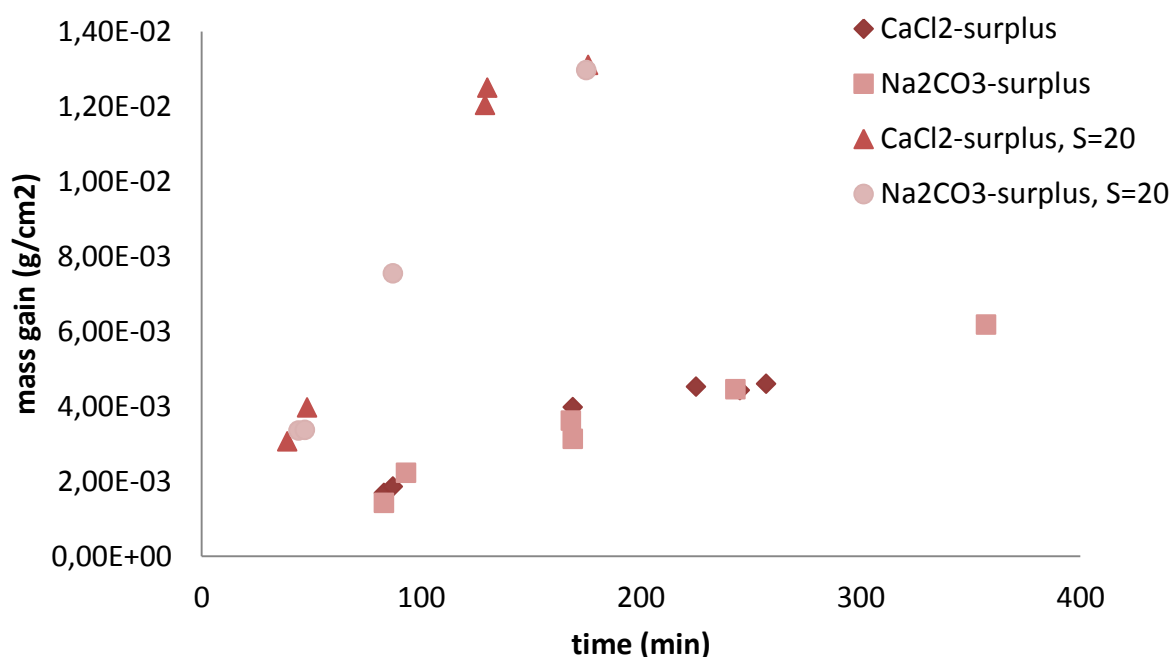Figure 47: Mass gain as function of time (S=6, Ttube=90, Tbulk=30)

In Figure 47, the data presented in Figure 42 is differentiated on the surplus reactant. As seen, no systematic difference in scale deposition was found due to the relatively small deviation from stoichiometric conditions. Stoichiometric conditions were therefore assumed when performing calculations on the supersaturation in the reactor.

C   Experimental uncertainty

All measurements have a certain uncertainty, which will propagate to the calculated result. Errors can be systematic around a different value than the true mean. This is often a result of poor calibration, inaccurate reading of measurement devices, noise, lack of sensitivity and similar. Systematic errors are possible to identify and eliminate.

Random errors are errors which vary without system around the true mean. Such errors are not always possible to eliminate. Statistical treatment can be used to extract information from measurement with random errors. In order to reduce the errors, the experiments should be repeated in order to get as close to the true mean as possible.

There are many ways to express the uncertainty. If the uncertainty for each measurement is known, an overall propagated error can be estimated. If some of the uncertainties are unknown or hard to estimate, as in this work, another way of estimating uncertainty should be used. One way is to lump all the uncertainty from the different measurement into one number, which is calculated from the final output. In order to do so, an average is estimated. If we have n measurements of the output x, the average is given as:

$$\overline{x} = \frac{1}{n}\sum_{i=1}^{n} x_i$$

Based on this average, a standard deviation can be calculated using this formula:

$$s \equiv \sqrt{\frac{1}{n-1}\sum_{i=1}^{n}(x_i - \overline{x})^2}$$

Another way to express errors is to use the maximum error method:

$$\Delta x_{max} = \frac{x_{max} - x_{min}}{2}$$

No measurements should ever fall outside the maximum error(Wolfs).

In Table 9 below, the experimental uncertainty for the scale growth rate experiments are summarized. The experiment length is directly related to the pump capacity deviation described in Appendix B and hence, given as maximum errors. The scale growth rate is calculated from the mass gain, experiment length and the area of the tube available for scaling. Here, the uncertainty is given as the standard deviation for each of the repeated experiment lengths. The average and standard deviation is calculated by Excel using the built-in version of the formulas above.

S	Number of experiments (n)	Average time (min)	Max error	Average scale growth rate (m/s)	Standard Deviation
6	4	87	6 %	4,20E-09	14 %
	3	169	0 %	4,34E-09	12 %
	4	243	7 %	3,80E-09	6 %
	1	357	0 %	4,34E-09	0 %
20	4	45	10 %	2,17E-08	6 %
	1	87	0 %	2,43E-08	0 %
	2	130	0 %	2,65E-08	2 %
	2	176	0 %	2,08E-08	0 %

In Figure 48and Figure 49, the data from the scale growth rate experiments are shown together with the statistical data given in Table 9.
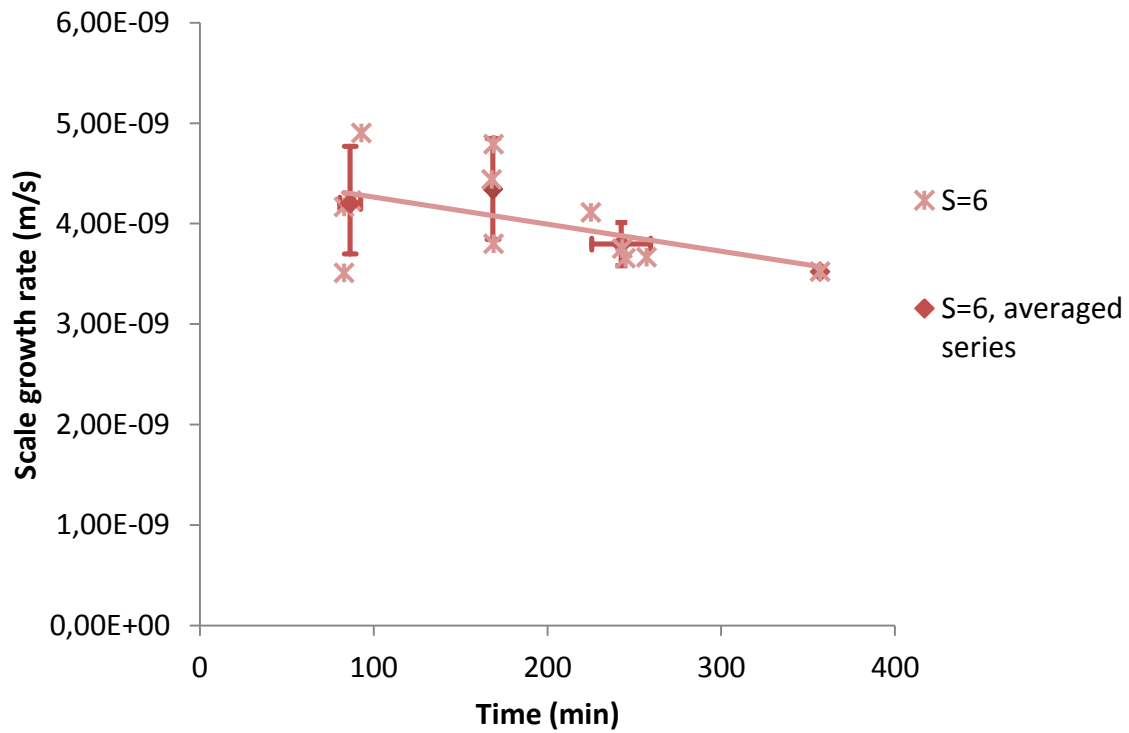
Figure 48: Data, average and standard deviation (S=6, Ttube=90, Tbulk=30)
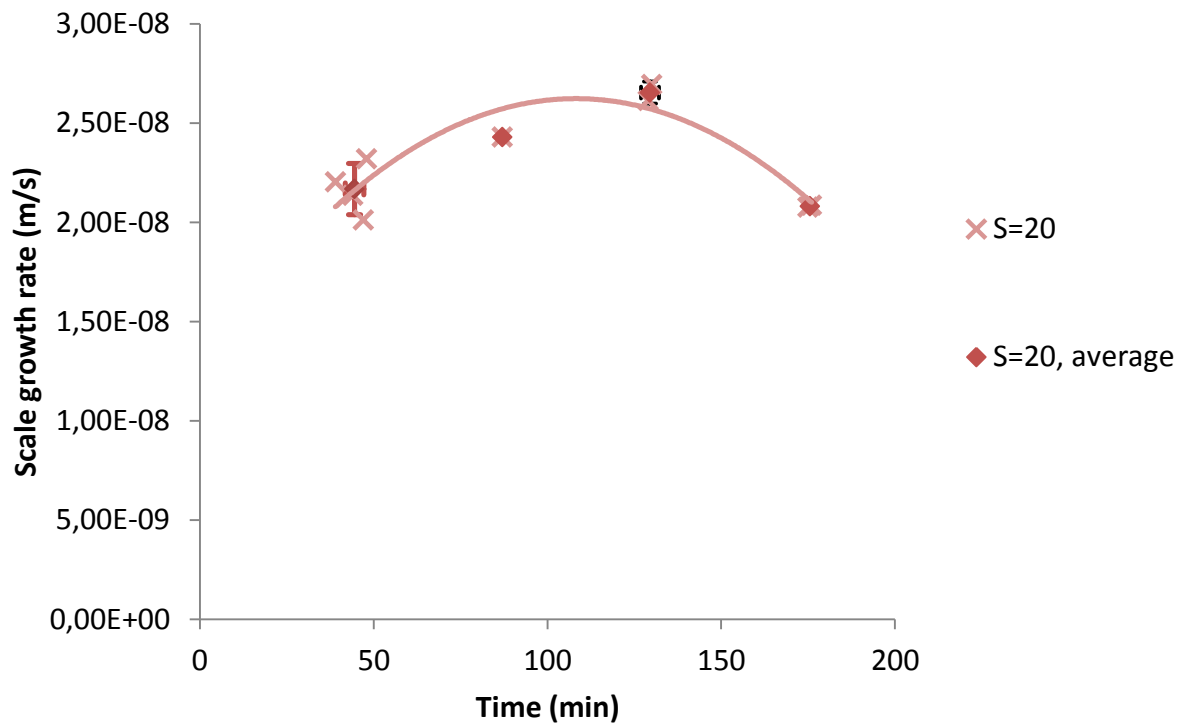
Figure 49: Data, average and standard deviation (S=20, Ttube=90, Tbulk=30)

From these figures, it is evident that the standard deviation is greatest for the shortest experiments and decreases as the experiments are prolonged. Also, the uncertainty is greater for experiments conducted at low supersaturations than at high. The error related to experiment length does not seem to impact the mass deposition to any significant extent.

As seen in Chapter 0, the deposited mass increases with supersaturation and experiment length. Thus, the error in scale growth rate can partly be explained by the difference between introductory and steady scale growth phase. As more mass is deposited, the system gets less sensitive to when the onset of steady growth occur.

D   Calculations

From MultiScale, the required concentration is given as $\frac{mmol}{kg}$. In order to find the necessary mass, following calculation is done:

$$m_{A,added}[g] = C_A\left[\frac{mmol}{kg_{solvent}}\right]\cdot\left[\frac{mol}{1000\cdot mmol}\right]\cdot M_A\left[\frac{g}{mol}\right]\cdot X_{tot}\left[kg_{solvent}\right]$$

Here, the amount of solvent is the total amount of solvent for both reactants, $X_{tot} = X_A\left(kg_{solvent}\right) + X_B\left(kg_{solvent}\right)$ as the reactants upon mixing will be miscible in both solvents, using both the available water amounts to be dissolved in,

After weighing out the necessary amounts, the actual concentration can be calculated in the same way:

$$g_{added}\cdot\left[\frac{1}{x_{kgsolvent}}\right]\cdot\frac{1}{M}\left[\frac{1}{g/mol}\right] = c\left[\frac{mol}{kg_{solvent}}\right]$$

$$n_{initial}[mol] = c\left[\frac{mol}{kg_{solvent}}\right]\cdot X\left[kg_{solvent}\right]$$

However, due to the inconsistent pumps as described in Appendix B , the solvent amount must be corrected for the actual amount of solution added:

$$X_{A,solvent,initially} - X_{A,left} = X_{A,added}$$

$$\frac{X_{A,added}}{X_{A,initial}} = \gamma\text{(fraction of reactants)}$$

$$\gamma\cdot n_{A,initial} = n_{A,added}$$

Now, the amounts of moles actually added are identified. In order to determine the actual concentration, the amount of solvent used must be taken into account. Similar as for component A:

$$X_{B,solvent,initially} - X_{B,left} = X_{B,added}$$

$$X_{tot,added} = X_{B,added} + X_{A,added}$$

As the actual amount of solvent used is known and the actual amount of moles added, it is possible to calculate a corrected concentration:

$$C_{A,corrected} = \frac{n_{A,added}}{X_{tot,added}}$$

$$C_{B,corrected} = \frac{n_{B,added}}{X_{tot,added}}$$

Throughout this work, the experimental results are presented as mass per area, mass deposition rate and linear growth rate. Mass deposition rate is calculated as follows:

$$\text{mass deposition rate} = \frac{1}{A}\frac{dW}{dt}\left[\frac{kg}{m^2 \cdot s}\right] = \frac{m[g]}{A[cm^2] \cdot t[s] \cdot \left[\frac{min}{60 \cdot s}\right]} \cdot \frac{\left[\frac{kg}{1000g}\right]}{\left[\frac{m^2}{10000cm^2}\right]}$$

In order to calculate the linear growth rate the estimated density is required. This is calculated as:

$$\rho\left[\frac{g}{cm^3}\right] = \frac{m[g]}{A[cm^2] \cdot L[cm]}$$

When the density is known, the linear rate can be determined:

$$\text{linear rate} = \frac{dL}{dt}\left[\frac{m}{s}\right] = \frac{\text{mass deposition rate}\left[\frac{g}{cm^2 \cdot s}\right]}{\rho\left[\frac{g}{cm^3}\right]} \cdot \left[\frac{m}{100cm}\right]$$

E   Tubes surfaces: area and impact on morphology

The surface areas of the heated tubes were estimated as follows:

Three straight pieces of the tube material was measured with a digital measuring device (3 digits on centimeter) and weighed on a fine scale (4 digits on gram). From these measurements and the tube diameter (0.25 inch, as given by the manufacturer), an average density surface density was calculated as

$$\frac{m[g]}{A\left[cm^2\right]} = \frac{m[g]}{L[cm] \cdot d[cm] \cdot \pi}$$

Each U-tube was than weighed and the surface area determined by dividing the mass on the surface density. 15 mm of each tube leg were covered by a silicone hose (in order to fasten the tube to the reactor lid). This area was subtracted from the total area, as scale would not form at this area.

$$\text{scaling area} = \frac{m[g]}{\rho\left[g\middle/cm^2\right]} - 1.5[cm] \cdot d[cm] \cdot \pi$$

The surface areas estimated are listed in Table 10 below.

Table 10: Tube surface area

Tube name	Weight [g]	Area [cm^2]	Covered area [cm^2]	Scaling area [cm^2]
DMV	30,9	53,2	1,0	52,2
Prikk	32,7	54,2	1,0	53,3
Fulltekst	30,8	50,9	1,0	50,0
Stjerne	32,0	52,9	1,0	52,0
Svartkant	30,6	50,7	1,0	49,8
Rille	33,0	54,6	1,0	53,7
Askrap	33,1	54,8	1,0	53,9
A	32,3	53,5	1,0	52,6
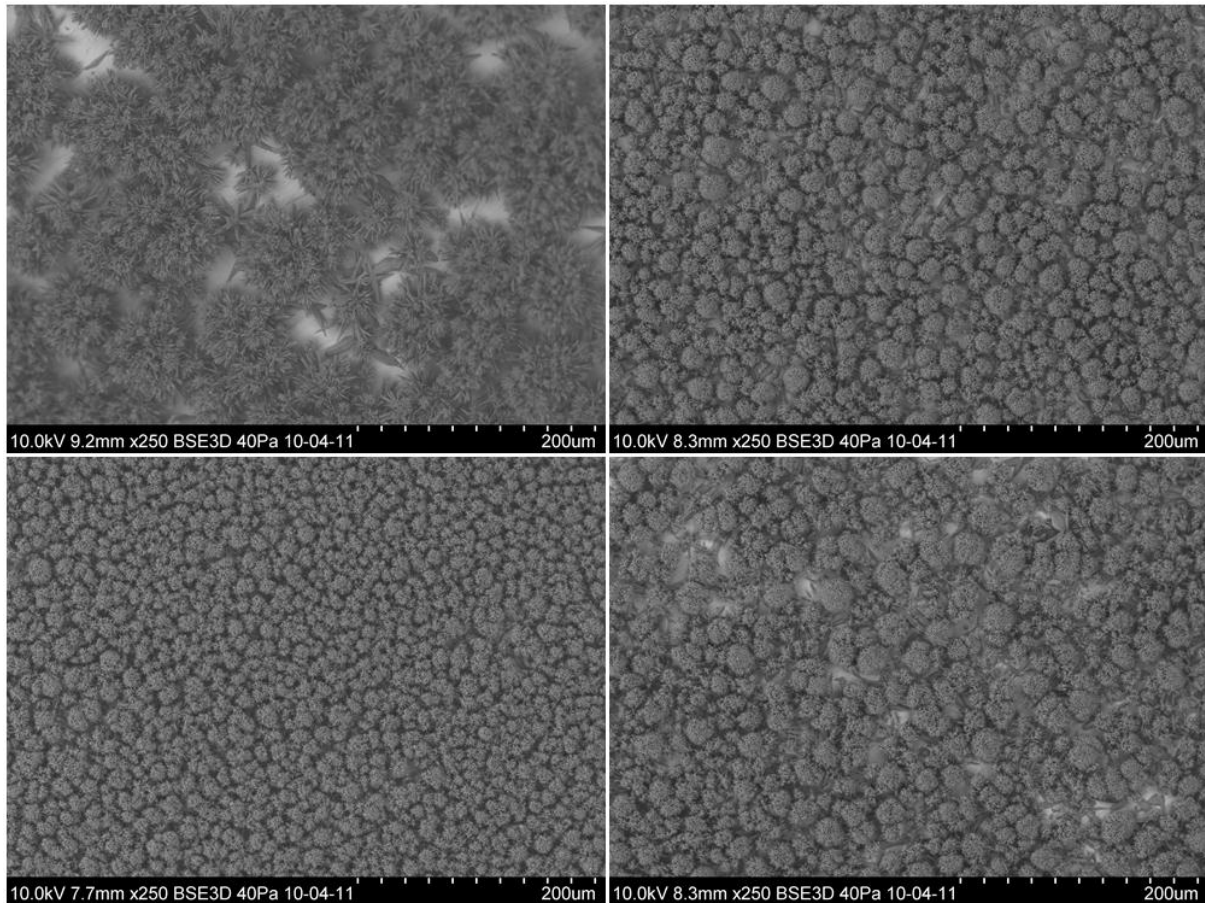
Figure 50: Surface scale variations at S=6, T_{tube}=90°C, T_{bulk}=30°C, 90 min

Between the different experiments conducted, only small deviations were found in the morphological appearance of the crystalline matter. However, as seen in Figure 50, one clear exception is seen. In the experiments at these conditions (S=6, Ttube=90°C, Tbulk=30°C, 90min), the crystal agglomerates are in the size range 10-30μm. For the experiment run with the tube "DMV", the agglomerate size is 60-80μm.

A comparison two experiments run with the "DMV"-tube and two experiments run with other tubes, indicates the same: The crystalline agglomerate at this surface are about 3 times larger than at other surfaces. This indicates that the surface of the tubes can impact the morphology of the growing polymorph. With regards to mass gain, the "DMV"-tube does not deviate from the other tubes and thus, the experiments run with the "DMV"-tube are not excluded from this study. But, this study is too limited to conclude that the mass deposition always will be unaffected by the surface. Rather, this discovery highlights the importance of a more systematic study of the influence of different surfaces on scale growth phenomena as rate morphology and stability.
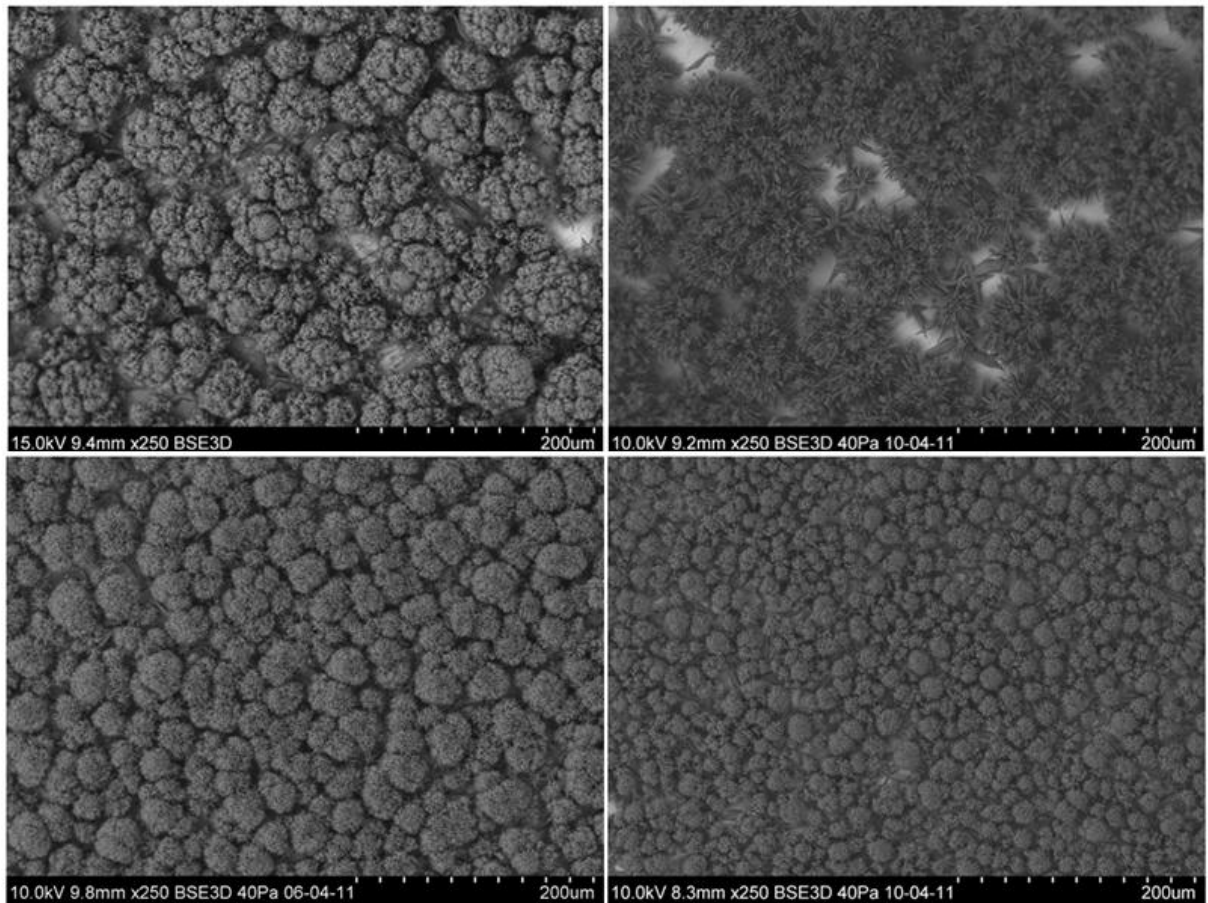
Figure 51: Upper row: "DMV"-tube after 180 min (left) and 90 min (right) Lower row: "A"-tube after 180 min (left), "Prikk"-tube after 90 min (right)

F   Supersaturation and calcium carbonate equilibria

The program MultiScale was used to calculate the amount of reactants required to obtain a desired supersaturation ratio at a given temperature. MultiScale is a multiphase equilibrium program which gives an accurate model for activity coefficients in aqueous solutions. The version used was Multi(MEG)Scale 7.0, which is developed for predicting scaling under influence of the antifreeze mono ethylene glycol (MEG) and widely used in industry (MultiScale, 2010).

In this appendix, details around the complexity of supersaturation are highlighted. Also, the calculations performed after obtaining a given concentration in MultiScale is presented.

Supersaturation is the ratio of the ionic activity product at present conditions to the ionic activity product at equilibrium (solubility product). For calcium carbonate, the supersaturation will vary with the different polymorphs: C

Ionic activity is temperature dependent through an Arrhenius relation. Also, it is sensitive to the presence of other ions. Several different supersaturations could have been used depending on whether the bulk temperature, the surface temperature, the initial concentrations or the steady state concentrations were used.

Table 11: Change in supersaturation for [CaCO3]=0.83mmol/kg with increasing temperature

Concentration (mmol/kg solvent)	Temperature (°C)	Supersaturation
0.84	30	6.3
	50	6.1
	70	5.9
	90	5.9

In Table 11 above, the supersaturation is calculated in MultiScale for a constant concentration. As shown, when temperature increases, the supersaturation actually gets slightly lower. This can be explained by the complete system of equilibria impacting the calcium-carbonate system. As temperature is increased, the kinetics of the system is impacted. Thus, reactions which are slow at room temperature might be significant at higher temperatures. To set a basis for the supersaturation and stick to this is therefore of great importance.

Following equilibria exist in the calcium carbonate system. The equilibria constants will change with temperature with an Arrhenius type of dependency. Also, pH will impact the equilibria constant.

Table 12: Calcium carbonate equilibria and equilibrium constants (taken from Parsiegla and Katz (1999))

Equilibrium reaction	Equilibrium constant (25°C, $I = 0$ M)
$H^+ + OH^- \rightleftharpoons H_2O$	$\log K_W = 14.00$
$CO_2(g) + H_2O \rightleftharpoons H_2CO_3^*$	$\log K_H = -1.47$
$HCO_3^- + H^+ \rightleftharpoons H_2CO_3^*$	$\log K_{HCO_3} = 6.35$
$CO_3^{2-} + H^+ \rightleftharpoons HCO_3^-$	$\log K_{CO_3} = 10.33$
$Na^+ + HCO_3^- \rightleftharpoons NaHCO_3^\circ$	$\log K_{NaHCO_3} = -0.25$
$Na^+ + CO_3^{2-} \rightleftharpoons NaCO_3^-$	$\log K_{NaCO_3} = 1.27$
$Na^+ + Cl^- \rightleftharpoons NaCl^\circ$	$\log K_{NaCl} = -0.5$
$Ca^{2+} + HCO_3^- \rightleftharpoons CaHCO_3^+$	$\log K_{CaHCO_3} = 1.05$
$Ca^{2+} + CO_3^{2-} \rightleftharpoons CaCO_3^\circ$	$\log K_{CaCO_3} = 3.15$
$Ca^{2+} + OH^- \rightleftharpoons CaOH^+$	$\log K_{CaOH} = 1.30$
$Ca^{2+} + Cl^- \rightleftharpoons CaCl^+$	$\log K_{CaCl} = 0.52$
$Ca^{2+} + CO_3^{2-} \rightleftharpoons CaCO_3(s)$ (calcite)	$\log K_{so} = 8.48$

G   XRD-analysis

In this work both qualitative and quantitative analyses are performed on the XRD-spectra. A short scan will give a rough pattern with less defined peaks and more background noise. However, such a scan is still useful to qualitative prove what compounds are present. As mentioned, the intensity of the peaks is related to crystallographic orientation, as well as the amount of the compound present which also will increase the intensity of the reflected beam. Hence, only looking at the intensity of the peaks will not give any information on what ratio the different compounds are present in.

Rough scans were analyzed by the software EVA. Here, scan patterns are uploaded and matched against the known patterns of compounds, taken from the database of the International Centre for Diffraction Data (2011). As seen in Figure 52, all three polymorphs of calcium carbonate are found both for experiments performed at S=6 and S=20.

To quantify the amount of the different polymorphs, long scans were performed. These scans gave more precise spectra, which allowed for analysis by TOPAS. This software uses the Rietveld method to refine a theoretical line to match a measured X-ray spectrum by using the least squares method. The function M is the difference between the calculated profile y_{calc} and the observed data y_{obs}

$$M = \sum_i W_i \left(y_i^{obs} - \tfrac{1}{c} y_i^{calc} \right)^2$$

where Wi is the statistical weight and c a scale factor such that $y_{calc} = c y_{obs}$. The reflection profile y_i from the position $2\theta i$ can, for the assumed Gaussian distribution, be given as

$$y_i = I_k \exp\left[\frac{-4\ln(2)}{H_k^2} \left(2\theta_i - 2\theta_k \right)^2 \right]$$

Where H_k is the width at half-peak height, $2\theta k$ is the centre of the reflection and I_k the intensity of the reflection (determined from parameters including the structure factor discussed in Section 2.11.2).

TOPAS require input of crystallographic data for the different polymorphs investigated. These data are obtained from the database of the International Centre of Diffraction. The following dataset were used: 04-008-5421 (aragonite), 04-012-8072 (calcite) and 04-011-5985 (vaterite).

Qualitative XRD-spectra with refined lines are given in Figure 53.
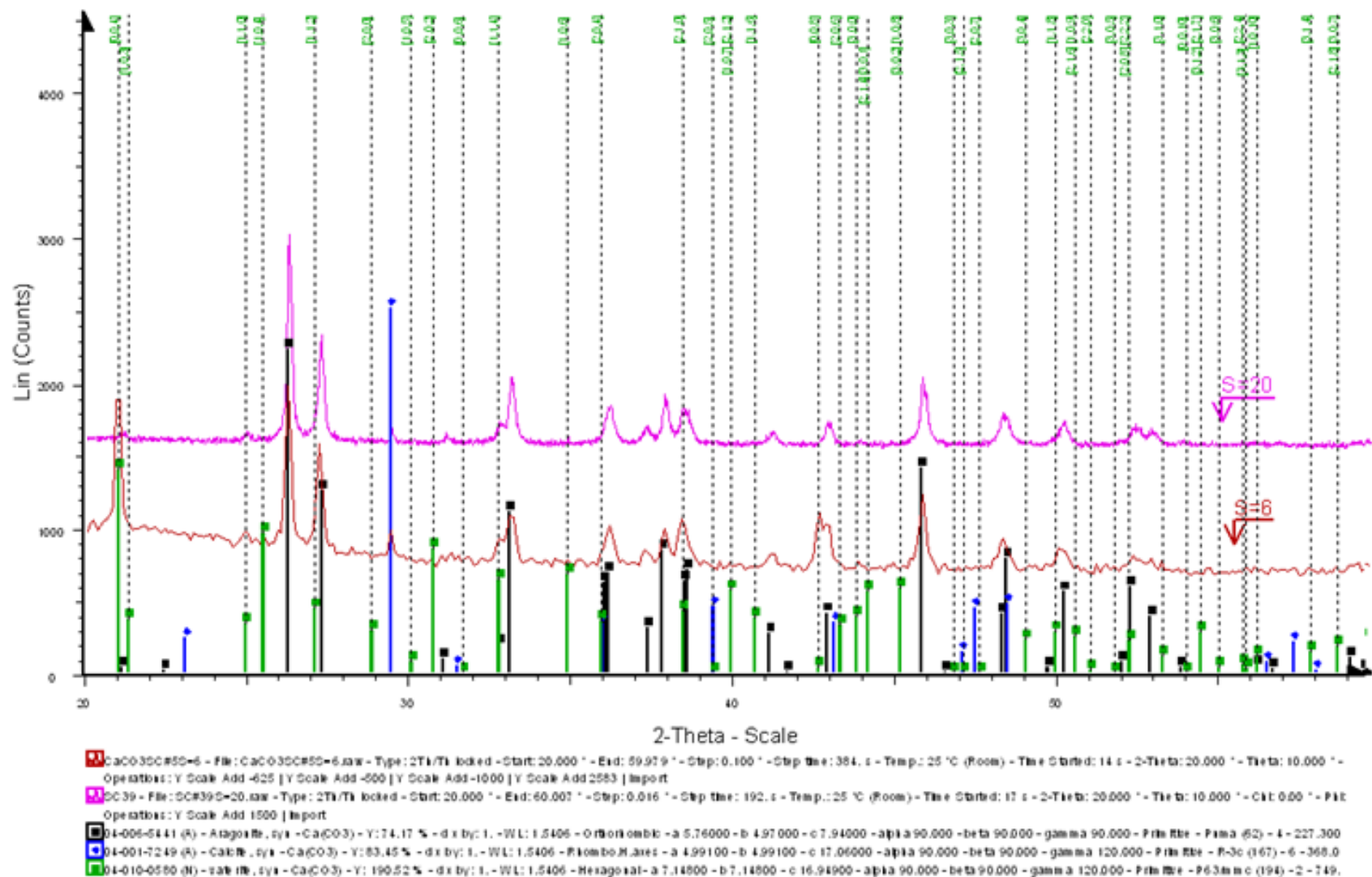
Figure 52: Qualitative XRD-scans for S=6 and S=20 revealing presence of all three polymorphs
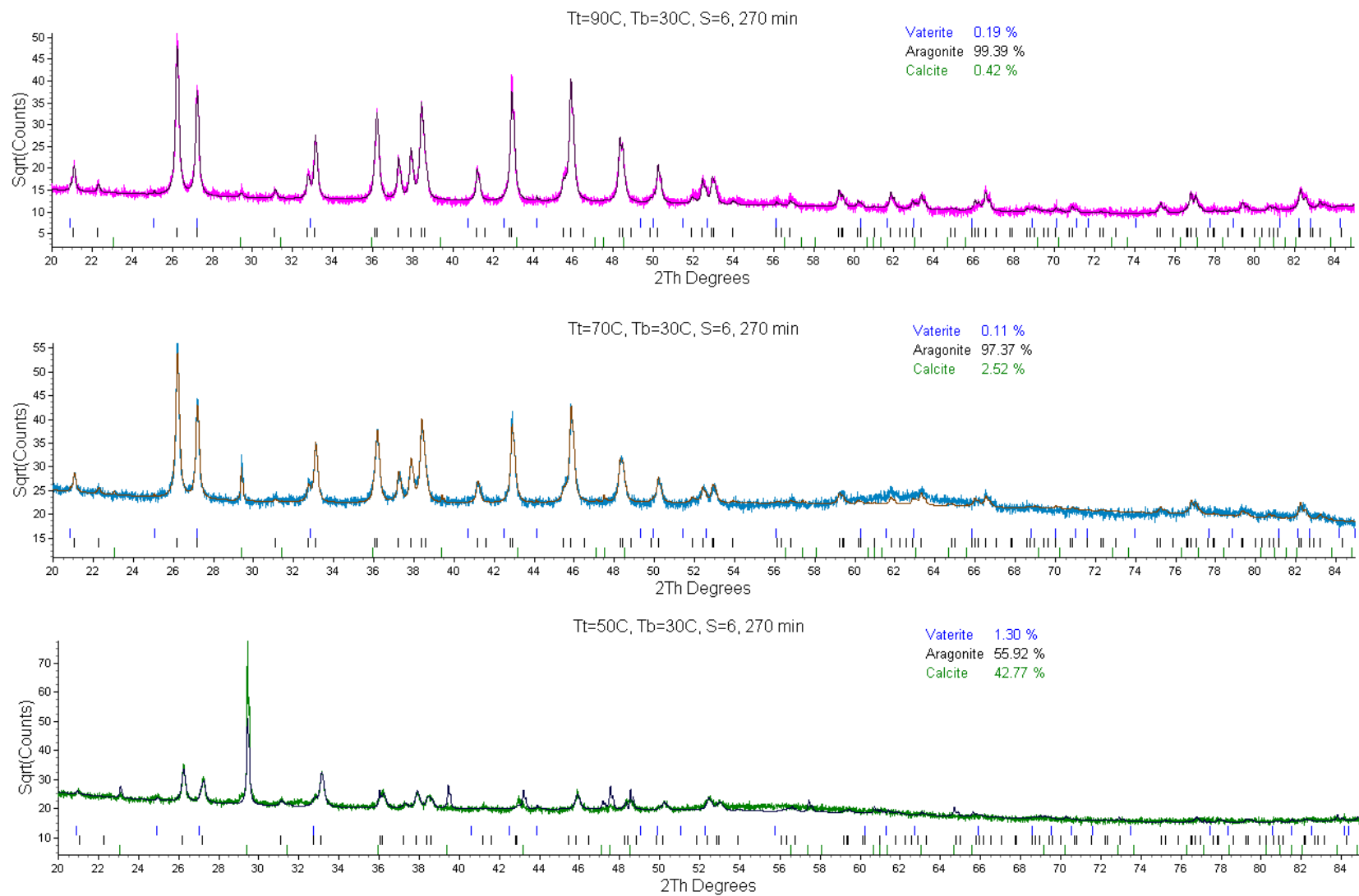
Figure 53: Quantitative XRD-spectra analyzed by Topas

H   Raw data

Experiment #	Tube	S actual	Tsurface [C]	Tbulk [C]	Residence time [1/min]	Corrected mass gain [g]	[m/s]	Mass gain per area [g/cm2]
18	Stjerne	8,4	90	30	3,10	0,084	3,82E-09	1,61E-03
18			90	30				
19	A	6,3	90	30	3,07	0,208	4,79E-09	3,96E-03
19			90	30				
20	Prikk	8,4	90	30	3,12	0,335	7,39E-09	6,29E-03
20			90	30				
21	A	5,3	90	30	3,26	0,649	2,81E-08	1,23E-02
21			90	30				
22	Prikk	4,3	90	30	3,04	0,011	2,44E-10	2,03E-04
22			90	30				
23	Stjerne	4,7	90	30	3,18	0,078	3,51E-09	1,49E-03
23			90	30				
24	A	6,3	90	30	3,08	0,165	3,80E-09	3,14E-03
24			90	30				
25	Rille	10,5	90	30	3,13	0,139	6,17E-09	2,59E-03
25			90	30				
26	Askrap	6,2	90	30	3,35	0,331	3,52E-09	6,14E-03
26			90	30				
27	Prikk	12,3	90	30	2,84	0,268	1,34E-08	4,99E-03
27			90	30				
28	Stjerne	6,3	90	30	2,72	0,235	4,11E-09	4,51E-03
28			90	30				

29	DMV	20,8	90	30	3,14	0,394	2,43E-08	7,30E-03
29			90	30				
30	Fulltekst	6,3	90	30	2,95	0,223	3,75E-09	4,45E-03
30			90	30				
31	Svartkant	6,2	90	30	3,02	0,218	3,66E-09	4,38E-03
31			90	30				
32	DMV	6,4	90	30	2,99	0,088	4,16E-09	1,69E-03
32			90	30				
33	Stjerne	6,4	90	30	3,11	0,093	4,23E-09	1,80E-03
33			90	30				
34	Prikk	6,4	90	30	2,97	0,076	3,51E-09	1,42E-03
34			90	30				
35	A	6,4	90	30	3,07	0,242	3,67E-09	4,60E-03
35			90	30				
36	Askrap	6,2	90	30	3,50	0,120	4,90E-09	2,23E-03
36			90	30				
37	Rille	20,8	90	30	3,15	0,695	2,08E-08	1,26E-02
37			90	30				
38	A	20,6	90	30	3,33	0,176	2,14E-08	3,35E-03
38			90	30				
39	Svartkant	20,6	90	30	3,33	0,168	2,01E-08	3,35E-03
39			90	30				
40	Prikk	20,8	90	30	3,18	0,698	2,09E-08	1,30E-02
40			90	30				
41	Stjerne	20,6	90	30	3,19	0,160	2,20E-08	3,07E-03
41			90	30				
42	DMV	20,6	90	30	3,19	0,208	2,32E-08	3,97E-03
42			90	30				
43	Prikk	20,9	90	30	3,10	0,666	2,69E-08	1,25E-02
43			90	30				

44	Fulltekst	20,9	90	30	3,10	0,602	2,61E-08	1,19E-02
44			90	30				
45	A	6,1	90	50	3,67	0,084	2,52E-09	1,58E-03
45			90	50				
46	Stjerne	6,4	90	50	3,67	0,196	4,33E-09	3,76E-03
46			90	50				
47	Fulltekst	6,4	90	70	3,00	0,211	5,22E-09	4,15E-03
47			90	70				
48	DMV	6,3	90	30	3,07	0,191	4,44E-09	3,62E-03
48			90	30				
49	Askrap	6,4	50	30	3,10	0,176	2,60E-09	3,27E-03
49			50	30				
50	A	6,4	50	30	3,16	0,054	2,39E-09	1,03E-03
50			50	30				
51	Rille	6,4	30	30	3,13	0,004	5,85E-11	7,45E-05
51			30	30				
52	Svartkant	6,2	70	30	3,27	0,216	3,41E-09	4,30E-03
52			70	30				
53	Fulltekst	6,4	50	30	3,11	0,076	3,56E-09	1,51E-03
53			50	30				
54	A	6,4	70	30	3,33	0,238	3,33E-09	4,53E-03
54			70	30				
55	Svartkant	6,4	70	30	3,25	0,096	2,18E-09	1,93E-03
55			70	30				
56	Askrap	6,4	70	30	3,57	0,281	3,60E-09	5,18E-03
56			70	30				
57	Rille	6,4	70	30	N/A	N/A	N/A	N/a
57			70	30				
58	Fulltekst	5,3	90	30	3,19	0,021	9,74E-10	4,14E-04
58			90	30				

59	Askrap	20,7	90	30	3,20	0,370	2,19E-08	6,87E-03
59			90	30				
60	Rille	6,3	90	30	3,35	0,403	4,24E-09	7,40E-03
60			90	30				
61	Svartkant	6,4	80	30	2,99	0,250	4,11E-09	5,02E-03
61			80	30				
62	Prikk	6,3	90	30	3,22	0,190	4,12E-09	3,56E-03
62			90	30				

I   HSE-forms

NTNU		Risikovurdering	utarbeidet av	Nummer	Dato	
⊙			HMS-avd.	HMSRV2603	4.3.2010	
HMS/KS			godkjent av	side	Erstatter	
			Rektor	1 av 1	9.2.2010	

Enhet: Diplomarbeid for Margrethe Nergaard   **Dato:** 24.06.2011
Linjeleder: Jens-Petter Andreassem
Deltakere ved risikovurderingen (m/ funksjon):

ID nr	Aktivitet fra kartleggings- skjemaet	Mulig uønsket hendelse/ belastning	Vurdering av sannsyn- lighet (1-5)	Vurdering av konsekvens:				Risiko- verdi	Kommentarer/status Forslag til tiltak
				Menneske (A-E)	Ytre miljø (A-E)	Øk/ materiell (A-E)	Om- dømme (A-E)		
	Søl av etsende kjemikalier (saltsyre)	Etseskade, øyeskade	3	C				3C	Alltid bruke øyevern, hansker samt utvise forsiktighet
	Søl av varmt vann (90°C) ved avhopp av slanger eller flytting av vannbad	Brannskade	4	B				4B	Sette opp skjerm som beskytter mot sprut dersom slangen hopper av. Flytte vannbad kun når de er slått av.
	Sette fast hår eller fingre i røremotorene	Sår	3	A				3A	Alltid ha hår oppsatt i strikk. Utvise forsiktighet når røremotorene er i gang.

Sannsynlighet	**Konsekvens**	**Risikoverdi (beregnes hver for seg):**
1. Svært liten	A. Svært liten	Menneske = Sannsynlighet x Konsekvens Menneske
2. Liten	B. Liten	Ytre miljø = Sannsynlighet x Konsekvens Ytre miljø
3. Middels	C. Moderat	Økonomi/materiell = Sannsynlighet x Konsekvens Øk/materiell
4. Stor	D. Alvorlig	Omdømme = Sannsynlighet x Konsekvens Omdømme
5. Svært stor	E. Svært alvorlig	

xx

Enhet: **Diplomarbeid for Margrethe Nergaard**   **Dato: 24.06.2011**
Deltakere ved kartleggingen (m/ funksjon):

Kort beskrivelse av hovedaktivitet/hovedprosess: Utførelse av laboratoriearbeid

ID nr.	Aktivitet/prosess	Ansvarlig	Lov, forskrift o.l.	Eksisterende dokumentasjon	Eksisterende sikringstiltak	Kommentar
	Generell labaktivitet rundt krystallisering av kalsiumkarbonat	Margrethe Nergaard				Innebærer liten risiko
I	Vask av labutstyr med fortynnet saltsyre.	Margrethe Nergaard		Datablad for saltsyre	Bruk av vernebriller, hansker og labfrakk	
	Bruk av mekanisk røreutstyr	Margrethe Nergaard			Utvise forsiktighet.	

NTNU		Handlingsplan for HMS	utarbeidet av	Nr.	dato	
			HMS-avd.	HMSRV12/24	04.03.2010	
⊙			Godkjent av	side	Erstatter	
HMS			Rektor	1 av 1	01.12.2006	

Enhet: _____**Diplomarbeid for Margrethe Nergaard**_____

Handlingsplan

ID.nr	Beskrivelse av tiltaket	Ansvarlig	Innen dato	Gjennomført/ Kontrollert, dato
	Ingen handlingsplan er påkrevd utover tiltakene beskrevet i risikovurderingen			

Dato: _____24.06.2011_____   **Linjeleder:** _____